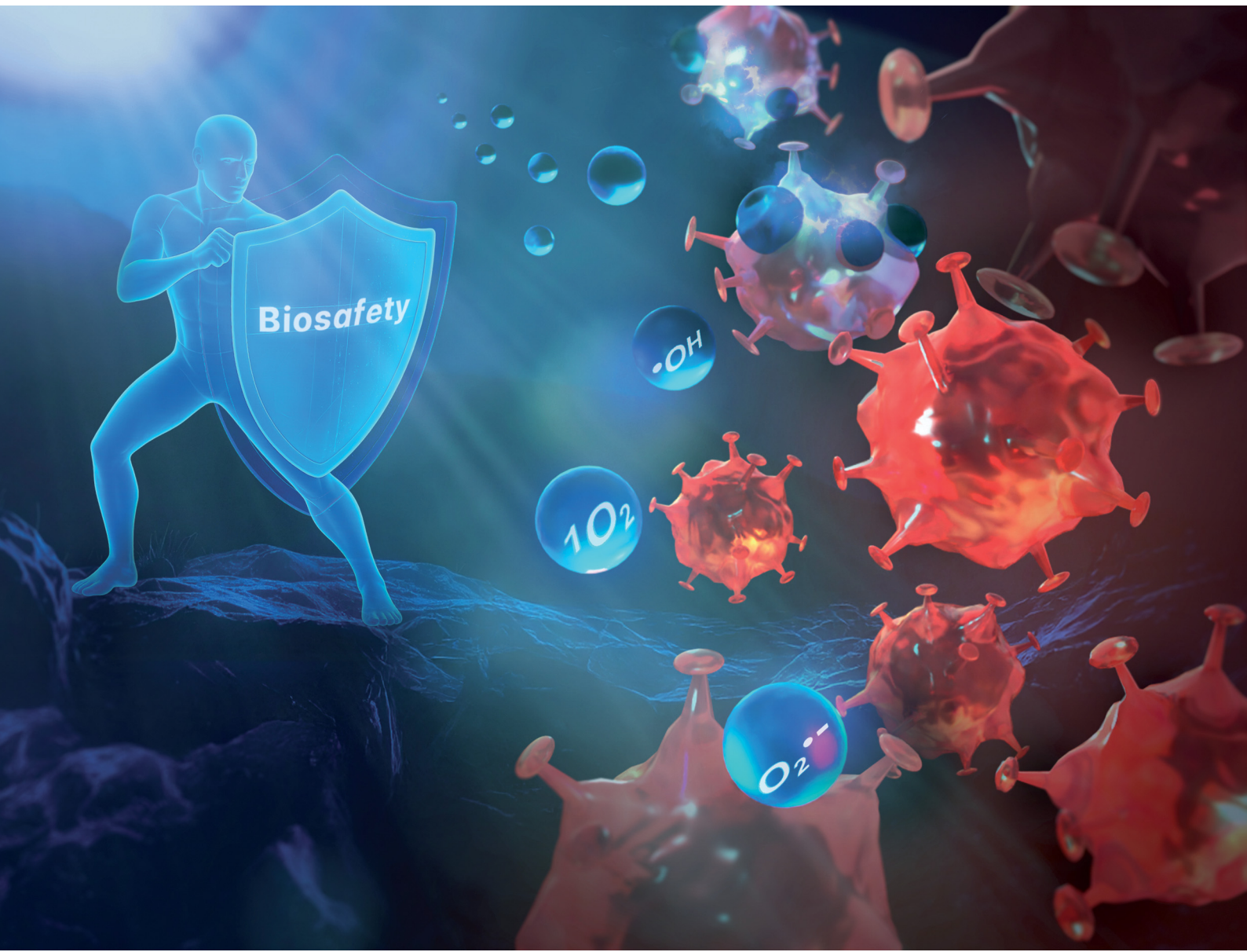


# Chem Soc Rev

Chemical Society Reviews

[rsc.li/chem-soc-rev](http://rsc.li/chem-soc-rev)



ISSN 0306-0012



Cite this: *Chem. Soc. Rev.*, 2025, 54, 7749

## Enhancing biosafety in photodynamic therapy: progress and perspectives

Yuan-Yuan Zhao,<sup>†,ab</sup> Lu Lu,<sup>†,c</sup> Hyunsun Jeong,<sup>†,b</sup> Heejeong Kim, <sup>†,b</sup> Xingshu Li, <sup>†,a</sup> Hua Zhang<sup>\*,c</sup> and Juyoung Yoon <sup>†,bd</sup>

Photodynamic therapy (PDT), a non-invasive method with minimal drug-resistance, high spatiotemporal selectivity, and involvement of reactive oxygen species (ROS) in phototherapy methods, plays an increasingly vital role in cancer treatment. Throughout the development of PDT, enhancing the therapeutic efficacy of photosensitizers (PSs) has been a consistent research focus. However, the continuous progress and widespread use of PDT have highlighted the importance of its safety. For instance, the significant side effects of PSs remain a notable issue, given that traditional PSs utilize an "always-ON" strategy, leading to severe phototoxic symptoms such as burning sensations, skin redness, and scabbing. Furthermore, patients must avoid natural light exposure for several weeks post-treatment. Additionally, attention should be directed towards the metabolism and clearance pathway, a critical pharmacokinetic feature that eliminates unwanted materials from the body post-treatment to prevent toxicity and damage. This review summarizes recent developments in smart PSs that exhibit highly effective cancer therapeutic functions with enhanced biosafety, addressing the inconveniences faced by patients following conventional PDT. In addition, the review discusses the challenges and future prospects for promoting the increasing application of PDT in clinical practice.

Received 9th June 2025

DOI: 10.1039/d5cs00054h

rsc.li/chem-soc-rev

### Key learning points

- The basic concepts and significance of photodynamic therapy.
- The significance of photosensitizers in photodynamic therapy.
- The advantages of photosensitizers with high safety in biomedical applications.
- Recent developments in constructing smart photosensitizers to enhance the safety of photodynamic therapy.
- Current challenges and future developments of clinical photodynamic therapy.

## 1. Introduction

Photodynamic therapy (PDT) is a promising technology for cancer treatment that has been extensively studied in the past decade. PDT systems typically consist of three essential components: molecular oxygen ( $O_2$ ), appropriate light or laser

exposure, and a photosensitizer (PS).<sup>1–4</sup> When exposed to light, the PS absorbs energy and transfers it to the surrounding  $O_2$ , producing various reactive oxygen species (ROS) *in situ*, such as singlet oxygen ( $^1O_2$ ), hydroxyl radicals ( $OH^\bullet$ ), and superoxide radicals ( $O_2^\bullet-$ ). These ROS can effectively eliminate cancer cells and achieve the desired treatment outcomes.<sup>5,6</sup> Compared to conventional treatment methods such as radiotherapy and chemotherapy, PDT offers several advantages, including precise spatial and temporal control, minimal drug resistance, and non-invasiveness.<sup>7–9</sup> Specifically, PDT shows promise in combination with other therapies, such as chemotherapy and photothermal therapy (PTT), to enhance treatment efficacy.<sup>10–20</sup> In addition, PDT can stimulate robust anti-tumor immune responses, which help prevent tumor recurrence and metastasis.<sup>21–24</sup>

As the central component in PDT, the inherent performance of PSs determines the treatment effectiveness. Therefore,

<sup>a</sup> Fujian Provincial Key Laboratory of Cancer Metastasis Chemoprevention and Chemotherapy, College of Chemistry, Fuzhou University, Fuzhou, 350108, China. E-mail: xingshuli@fzu.edu.cn

<sup>b</sup> Department of Chemistry and Nanoscience, Ewha Womans University, Seoul 03760, Republic of Korea. E-mail: jyoon@ewha.ac.kr

<sup>c</sup> Henan International Joint Laboratory of Smart Molecules and Identification and Diagnostic Functions, School of Chemistry and Chemical Engineering, Henan Normal University, Xinxiang, 453000, China. E-mail: zhh1106@htu.edu.cn

<sup>d</sup> Graduate Program in Innovative Biomaterials Convergence, Ewha Womans University, Seoul 03760, Korea

<sup>†</sup> These authors contributed equally to this work.



substantial efforts have been made to enhance the generation of ROS by PSs for efficient PDT.<sup>24–29</sup> Various approaches have been employed to enhance the ROS production capacity of PSs, such as Förster resonance energy transfer (FRET)<sup>30–32</sup> and the heavy atom effect.<sup>33–35</sup> Additionally, diverse strategies have been devised to increase the concentration of PSs at tumor sites. These strategies include incorporating targeting groups into PSs, developing nanodrug-based systems to exploit the enhanced permeability and retention (EPR) effect, and utilizing proteins as carriers within the body.<sup>36–38</sup> Consequently, a large number of PSs, including inorganic PSs (*e.g.*, gold nanomaterials, metallic oxide, and carbon nanotubes),<sup>39–42</sup> organic PSs (*e.g.*, phthalocyanines, BODIPY, cyanines, and aggregation-induced emission fluorogens),<sup>7,43–49</sup> and polymer agents have been developed for PDT investigations.<sup>50–52</sup>

The majority of PSs used in clinical and preclinical research typically employ an “always ON” strategy, leading to potential ROS leakage before and after treatment.<sup>35,53–55</sup> Additionally, most reported PSs lack tumor specificity and have undesired pharmacokinetics.<sup>56–58</sup> These drawbacks compromise therapeutic efficiency and can result in phototoxic symptoms such as skin allergies, skin burns, and systemic sensitization, limiting the further application of these PSs.<sup>59–62</sup> Taking the clinically available first-generation PS, photofrin, as an example, the

residue drug after treatment is metabolized and eliminated slowly and remains in the physical environment (*e.g.*, skin, liver, and eyes) for a long time, inevitably resulting in cutaneous toxicity upon exposure to natural light.<sup>63</sup> According to the U.S. Food and Drug Administration (FDA) guidelines,<sup>64</sup> patients receiving this drug must avoid direct exposure of their eyes and skin to natural light for at least 4 weeks or more to prevent adverse effects, which can significantly disrupt their daily lives. Therefore, it is envisaged that if these side effects can be decreased, it would certainly facilitate the application of PSs in clinical practice.

In recent years, several research articles have addressed the development of the multifunctional PSs to improve treatment efficacy while enhancing treatment biosafety. However, to the best of our knowledge, no systematic discussion has focused on constructing smart PSs to reduce the side effects of PDT and enhance the biosafety pre- and post-PDT. To enhance the PDT biosafety and broaden PSs’ treatment applications in clinical practice, we present a review of recent advances in developing diverse smart PSs for biosafe photodynamic applications. This review focuses on summarizing strategies to mitigate PDT side effects and improve safety. Finally, we explore the future challenges and prospects of PSs as biomedical drugs for clinical PDT (Fig. 1).



**Yuan-Yuan Zhao**

*Yuan-Yuan Zhao received his PhD degree from the Fuzhou University in 2021 under the supervision of Prof. Jiandong Huang and Prof. Xingshu Li. Then he joined Prof. Juyoung Yoon's group as a post-doctoral researcher. His current interests include the design and development of activatable photosensitizers, nanoprobes, and multi-functional theranostic agents.*



**Lu Lu**

*Lu Lu is currently studying for her PhD at the School of Chemistry and Chemical Engineering, Henan Normal University. Her research is based on the use of naphthalimide molecules in cancer therapy.*



**Left to right: Hyunsun Jeong and Heejeong Kim**

*Hyunsun Jeong earned her BS degree at Ewha Woman's University, and continued her Master's study from 2022 at Ewha Womans University. Her main research interest is organic fluorescent materials for theranostics.*

*Heejeong Kim obtained her BSc from Ewha Womans University in 2020. Currently, she is pursuing her PhD degree under the supervision of Prof. Juyoung Yoon at Ewha Woman's University. Her research interest is focused on supramolecular nanoagents and AIE theranostic agents.*



## 2. PDT biosafety enhancement by activatable PS

Traditional PSs are designed for continuous cytotoxicity but have limitations, including poor tumor specificity, potential phototoxicity, and an inability to respond to biomarkers, thus restricting their further clinical applications. Pathological sites have a distinct microenvironment characterized by hypoxia,<sup>5,65,66</sup> low pH,<sup>61,67,68</sup> enzyme overexpression,<sup>69,70</sup> and elevated levels of hydrogen peroxide ( $H_2O_2$ ) and glutathione (GSH).<sup>25,71–73</sup> This unique microenvironment facilitates the development of activatable PSs for precise PDT. Activatable PSs maintain their photoactivity in the “OFF” state in normal tissues but can be activated to induce photodynamic activity in cancerous or diseased areas (Fig. 2a). Significantly, such activatable PSs developed in response to cancer-specific endogenous stimuli can improve the precision and tumor eradication efficiency of PDT. They function by regulating the

spatiotemporal activation of PSs, thereby minimizing potential side effects on normal tissues. For instance, the hypoxia-responsive tumor prodrug AQ4N is specifically activated under hypoxic conditions within tumors, where it releases its cytotoxic effects. This targeted activation enables the selective and safe treatment of hypoxic tumors.<sup>74</sup> Therefore, activatable PSs that can respond to tumors or other disease biomarkers play a crucial role in cancer treatment. Here, we highlight recent advancements in the development of phototheranostic agents that utilize activatable strategies to minimize off-target toxicity by activating only at tumor sites.

### 2.1. Single activatable PSs

Hypoxia is a prominent feature of most solid tumors, attributed to the rapid and invasive growth of tumor cells and abnormal angiogenesis.<sup>75,76</sup> Given this special feature of tumor microenvironments, Urano and colleagues investigated hypoxia as a stimulus for developing activatable PSs for PDT.<sup>77</sup> They developed a novel PS (azoSeR, Fig. 2b) by incorporating an azo group into the conjugated system of a seleno-rosamine dye. This modification effectively prevented the intersystem crossing (ISC) process, thus inhibiting the generation of  $^1O_2$  under normoxic environments. However, under hypoxic conditions, the azo group was reductively cleaved in cells (even at 5%  $O_2$  concentration), leading to intracellular generation of  $^1O_2$  and cell death. Consequently, azoSeR exhibited selective phototoxicity towards hypoxic cells while minimally affecting cells under a normoxic environment, showing promise for cancer treatment with reduced side effects. In a separate study, Zhou *et al.* developed a hypoxia-activated self-destructive paclitaxel prodrug (PTX<sub>2</sub>-Azo). Under hypoxic environments, PTX<sub>2</sub>-Azo underwent bioreduction, followed by sequential 1,6-elimination and decarboxylation reactions, ultimately producing the active chemotherapeutic drug PTX.<sup>78</sup> To achieve controlled activation, PTX<sub>2</sub>-Azo was coated with a peptide copolymer modified with the commercial PS chlorin e6 (Ce6) to form Ce6/PTX<sub>2</sub>-Azo



**Xingshu Li**

*photosensitizers and theranostic agents for bioimaging and therapy.*

*Xingshu Li received his PhD from Fuzhou University in 2015. From 2016, he worked as a post-doctoral fellow at Ewha Woman's University for 3 years, and then moved to the University of Toronto in 2019. After completing post-doctoral research, he joined Fuzhou University in 2020, where he is currently a Minjiang Distinguished Professor of the College of Chemistry. His current interests include the design and development of innovative*



**Hua Zhang**

*the Natural Science Foundation of China for Outstanding Young Scholars. Prof. Zhang has co-authored over 50 peer-reviewed papers and is a co-inventor of 10 patents.*

*Hua Zhang received her PhD in 2013 from the Dalian University of Technology. She is a professor at Henan Normal University, where her research interests range from organic chemistry to analytical chemistry, and the synthesis of novel functional organic dyes for bioanalysis and imaging. She is committed to providing valuable analytical tools for disease monitoring, diagnostics and theranostics. In 2017, she received a grant from*



**Juyoung Yoon**

*Juyoung Yoon is a distinguished professor at the Department of Chemistry and Nanoscience, Ewha Woman's University. He received his PhD (1994) from Ohio State University and conducted his postdoctoral work at UCLA and Scripps Research Institute. His research interests include investigations of fluorescence imaging probes, phototherapy and theranostics. He has been listed as a highly cited researcher in chemistry since 2014.*



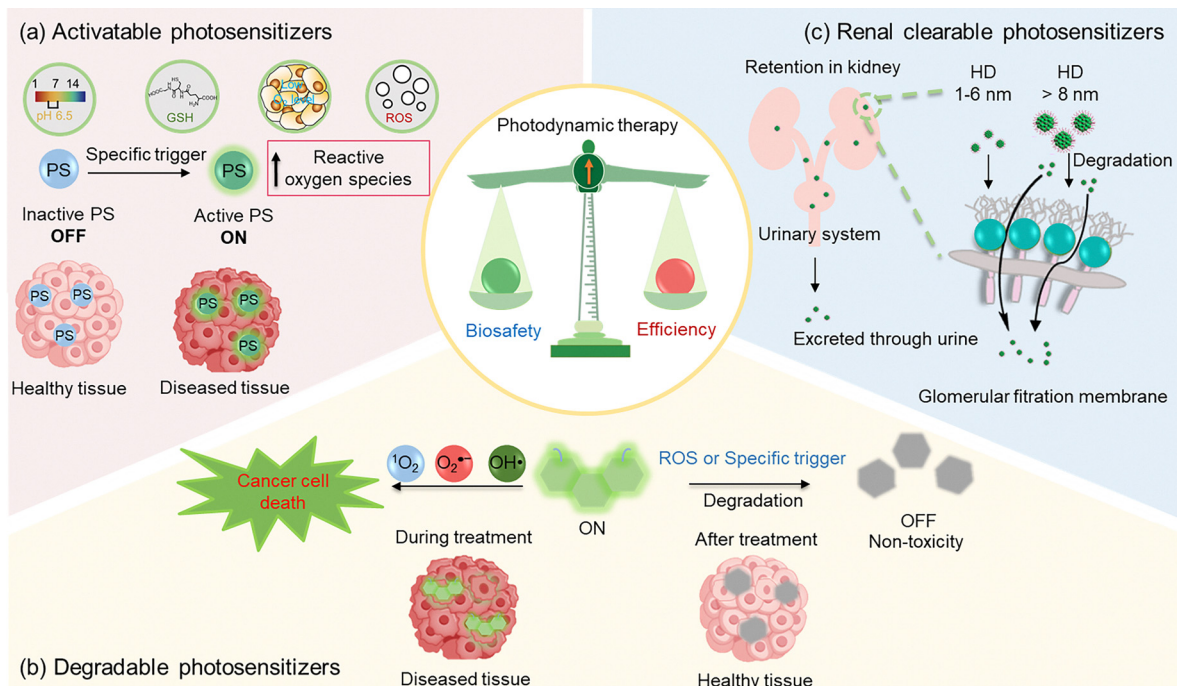


**Fig. 1** Schematic of the design principles of smart PSs, including (a) activatable, (b) degradable, and (c) renal-clearable PSs, to increase the efficacy of PDT while enhancing treatment biosafety.

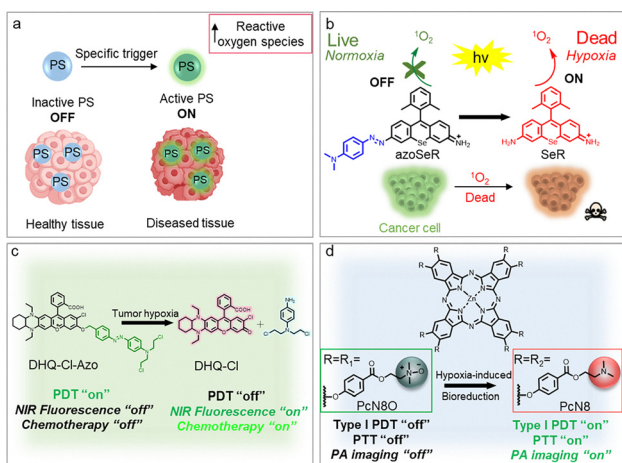


**Fig. 2** (a) Schematic of single-activatable PSs for enhanced safety of PDT. (b) Chemical structure of a representative PS (azoSeR) and its activated form in response to hypoxia. Reproduced with permission from ref. 77. Copyright, 2017, American Chemical Society. (c) Photodynamic effect response of DHQ-Cl-Azo in a hypoxic tumor environment. Reproduced with permission from ref. 79. Copyright, 2022, Elsevier. (d) Chemical structure of a representative PS (azoSeR) and its activated form under hypoxic conditions. R1 represents the *N*-oxide group. R2 represents the tertiary amine group. Reproduced with permission from the ref. 80. Copyright, 2025, John Wiley & Sons.

nanoparticles (NPs). In this formulation, the dimeric  $\text{PTX}_2\text{-Azo}$  not only significantly increased drug loading compared to its parent PTX but also prevented unintended drug release. Upon intravenous administration, Ce6/PTX<sub>2</sub>-Azo NPs accumulated at tumor sites due to the long circulation effect. In the hypoxic

tumor microenvironment, the Azo linker in  $\text{PTX}_2\text{-Azo}$  was partially cleaved, releasing PTX. Subsequently, under laser illumination, the co-encapsulated Ce6 was activated to produce  $^1\text{O}_2$  to cause cell apoptosis, while  $\text{O}_2$  consumption exacerbates hypoxia, further promoting PTX release. Ultimately, the released PTX can migrate to microtubules to interfere with cell division and synergize with  $^1\text{O}_2$  to inhibit tumor growth. Through this mechanism, the prepared Ce6/PTX<sub>2</sub>-Azo NP realized maximized therapeutic efficiency with negligible side effects. In 2022, Xiong and colleagues developed a molecular therapeutic agent (termed DHQ-Cl-Azo, Fig. 2c) that combines hypoxia-responsive PDT, chemotherapy, and near-infrared (NIR) fluorescence imaging for synergistic treatment of solid tumors.<sup>79</sup> This agent enabled potent PDT in normoxic tumor cells at the tumor periphery and triggered chemotherapy in the hypoxic core, effectively treating tumors. The tumor sizes and weights in the group treated with DHQ-Cl-Azo and 660 nm light irradiation were significantly smaller than those in other control groups, confirming that the hypoxia-activated chemotherapy and PDT strategy of DHQ-Cl-Azo can effectively inhibit tumor growth. Moreover, mice treated with DHQ-Cl-Azo and 660 nm light irradiation showed no obvious systemic toxicity, demonstrating excellent biosafety. This study introduces a novel strategy for designing hypoxia-responsive theranostic agents that integrate PDT and chemotherapy, holding great promise for cancer treatment with high biosafety.

In a recent report, Li and colleagues designed and synthesized a hydrophilic type I PS (PcN8O, Fig. 2d) with switchable characteristics that are activated exclusively in hypoxic tumor environments, utilizing the distinctive structural features of the



*N*-oxide group.<sup>80</sup> Specifically, *PcN8O* has the ability to form a uniform and stable nanoparticle (*NanoPcN8O*) in aqueous solutions through a spontaneous assembly process. *NanoPcN8O* can undergo facile bioreduction under hypoxic conditions to yield the product *NanoPcN8*, which contains abundant electron-rich tertiary amine groups. This activation triggers a type I photodynamic reaction, generating 4.1-times more  $\text{O}_2^{\bullet-}$  than the well-known PS methylene blue while also initiating a photothermal effect that produces significant heat. These properties resulted in a notable enhancement of the treatment response *in vivo*, effectively suppressing tumor growth through the combined effects of type I PDT and photothermal action without causing significant side effects. Importantly, *NanoPcN8O* is selectively activated in hypoxic tumors to produce type I ROS and heat during phototherapeutic treatment, remaining non-toxic in normal tissues. While the light excitation of the other “always-ON” PSs (*Ce6* and *NanoPcN8*) led to severe skin damage in the mice, the hypoxia-activatable *NanoPcN8O* caused minimal cellular damage to the skin tissues even under light irradiation, indicating favourable biosafety. This specificity minimizes the side effects and improves tumor specificity in PDT.

Tumor tissues have a distinct microenvironment characterized by slight acidity, as evidenced by the extracellular pH in normal tissues (pH 7.4), which is generally higher than that in tumor tissues (pH 6.5–7.2).<sup>81,82</sup> This phenomenon is attributed to enhanced glycolysis and plasma membrane proton pump activity in cancer cells, resulting in elevated lactate production.<sup>83</sup> Therefore, utilizing a compound that enhances ROS production under acidic pH while showing reduced activity at a pH value of approximately 7.4 can aid in achieving precise PDT with high biosafety. Based on this rationale, Zou *et al.* developed a phenyl-based boron dipyrromethene (BODIPY) derivative (*BDPtriPh*, Fig. 3a) by adding three diethylamino groups to the BODIPY core.<sup>84</sup> Importantly, the  $\text{^1O}_2$  generation and the photothermal conversion capacities monitored under different pH values revealed that the diethylamino groups in the synthesized BODIPY derivative could function as proton acceptors activated by the low pH in lysosomes, thereby enhancing the efficacy of PDT and PTT. To improve the dispersibility of *BDPtriPh* in aqueous solutions, *BDPtriPh* nanoparticles (*BDPtriPh NPs*) were prepared using a nano-precipitation approach. Encouragingly, *in vivo* fluorescence imaging demonstrated the remarkable tumor-targeting ability of *BDPtriPh NPs* because of the EPR effect. Ultimately, these advantages resulted in a significant improvement in the treatment response *in vivo*, effectively inhibiting tumor growth through the synergistic effects of PDT and PTT. Importantly, minimal damage was observed in normal tissues, including the kidneys, spleen, lungs, liver, and heart, indicating low dark toxicity as well as excellent biocompatibility.

Another pH-activated PDT system with high biosafety was developed by Lin and co-workers. As shown in Fig. 3b, they presented a series of pH-activated long-wavelength PSs (*LET-I*,  $R = H, Cl, Br, I$ ) based on cyanine dye.<sup>85</sup> These synthesized PSs initially adopt a ring-closed conformation, transitioning to a

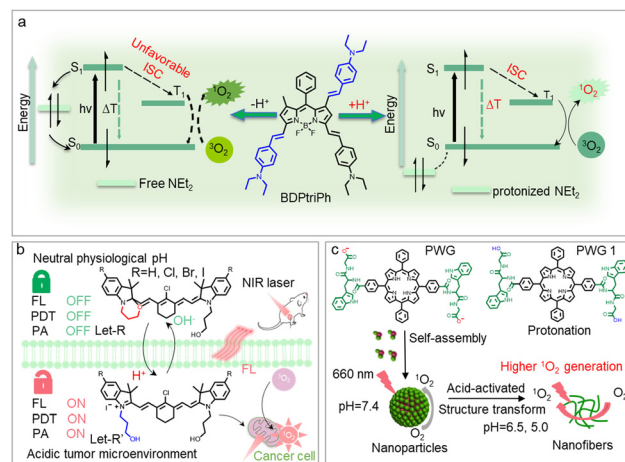


Fig. 3 (a) Photodynamic effect response of *BDPtriPh* in the mild acidic environment. Reproduced with permission from ref. 84. Copyright, 2019, Royal Society of Chemistry. (b) Chemical structure of a representative PS (*LET-I*) and its activated form under the mild acidic conditions. Reproduced with permission from ref. 85. Copyright, 2024, John Wiley & Sons. (c) Schematic of the self-assembly and fibrillar transformation of acid-activated peptide-porphyrin (PWG) nanoparticles and their application in PDT. Reproduced with permission from ref. 87. Copyright, 2020, John Wiley & Sons.

ring-open structure upon proton activation. This transition restores the cationic cyanine backbone, leading to strong long-wavelength absorption at 808 nm, particularly for *LET-I*. In addition, due to the significant promotion of ISC by the *I*, the  $\text{^1O}_2$  generation capacity of *LET-I* was significantly enhanced by 3.2-times compared to indocyanine green. These properties allow the folic acid-modified *LET-I* probe to realize complete photodynamic tumor eradication under ultra-low 808 nm laser power density ( $0.2 \text{ W cm}^{-2}$ ), aided by activatable photoacoustic and fluorescence dual-modal imaging. Moreover, minimal changes were observed in both major organs and blood chemistry during treatment, suggesting that *LET-I* effectively performs PDT while exhibiting good biocompatibility. This research offers valuable insights for developing tumor-specifically responsive therapeutic agents for precise PDT. In their continued innovative work in 2025, Lin's team developed another pH-responsive NIR hemicyanine-based PS (*LET-15*).<sup>86</sup> Similarly, *LET-15* can be activated in the acidic tumor microenvironment, targeting mitochondria and inducing cytotoxicity under laser irradiation. This selective action destroys tumor tissues while minimizing harm to normal tissue.

In 2020, Sun and co-workers developed an intriguing nano-system comprising a self-assembled peptide-porphyrin conjugate that selectively converts into active nanofibers for tumor suppression at pH 6.5 (Fig. 3c).<sup>87</sup> The peptide-porphyrin conjugate was synthesized by linking the pH-activated dipeptide tryptophan-glycine to a hydrophobic porphyrin core through amide bond formation. The dipeptide consists of glycine, providing carboxyl groups as an acid-sensitive fragment, and tryptophan, contributing delocalized  $\pi$  electrons for fluorescence. Importantly, the synthesized peptide-porphyrin conjugate can self-assemble under physiological conditions to form

nanoparticles. When the nanoparticles are enriched at tumor sites, the protonation of the peptide-porphyrin conjugate induced by increased acidity promotes the formation of intermolecular hydrogen bonds, resulting in the conversion of nanoparticles into nanofibers. Furthermore, histological examination of major organs, including kidneys, spleen, liver, and heart, revealed no significant histopathological changes following treatment. Utilizing this adaptable nanosystem, the peptide-porphyrin nanostructures demonstrated significant anti-tumor activity in PDT without off-target side effects.

As we are aware, GSH serves as an intracellular reductant utilized to combat oxidative stress and is prevalent in tumor cells due to their highly active metabolism.<sup>88,89</sup> Therefore, strategies aimed at targeting tumors with PDT can leverage the reactions involving GSH to enhance specificity. For instance, Wang and co-workers incorporated two photochemically inert precursors (MePy-N3 and TPA-alkyne-2<sup>+</sup>) into MOF-199 and then enveloped the precursor-laden MOF-199 with F-127, resulting in F127-loaded MOF-199 nanoparticles (PMOF NPs, Fig. 4a).<sup>90</sup> In this system, MePy-N3 and TPA-alkyne-2<sup>+</sup> were chosen for their ability to be synthesized into an aggregation-induced emission (AIE) PS (TPATrzPy-3<sup>+</sup>) through a click reaction catalyzed by Cu<sup>I</sup>, which is generated from GSH-reduced-MOF-199. After injecting PMOF NPs intravenously into tumor and cancer cells, Cu<sup>II</sup>-based MOF-199 within PMOF NPs was selectively reduced by GSH to produce Cu<sup>I</sup> in the cancer cells. Simultaneously, GSH-reduced PMOF NPs disintegrated to release the enclosed precursors (MePy-N3 and TPA-alkyne-2<sup>+</sup>), leading to the formation of the effective AIE PS (TPATrzPy-3<sup>+</sup>) through an intracellular click reaction facilitated by the generated Cu<sup>I</sup>. Upon exposure to light, the synthesized AIE PS TPATrzPy-3<sup>+</sup> could efficiently generate ROS within cancer cells, resulting in targeted cancer cell

ablation. Notably, the high specificity of such PS, which is exclusively generated within cancer cells, enhances the safety of post-treatment.

In the same year, Sun *et al.* developed an organic functional dye (named DANO, Fig. 4b), featuring a  $\pi$ -conjugated donor-acceptor (D-A) skeleton equipped with two amphiphilic triphenylphosphine ligands and one *N*-nitrosamine substituent.<sup>91</sup> The small *N*(Me)-NO substituent exerts a notable photocaging effect on the optical performances of the D-A motif through photoinduced electron transfer. The uncaging process can be co-regulated by GSH and light, stimulating multiple photochemical reactions after the release of  $\bullet$ NO. Additionally, the activated DANO acts as an efficient PS to produce ROS through both type I and type II photoreactions, as well as generate reactive nitrogen species (ONOO<sup>-</sup>) through secondary radical-participating reactions. The combination of cascade reactions and these collective features enable DANO to demonstrate outstanding *in vitro* PDT effects under both normoxic (21% O<sub>2</sub>) and hypoxic (1% O<sub>2</sub>) environments, effectively inducing cell apoptosis (<10% cell viability) even at an extremely low light power up to 6 J cm<sup>-2</sup>. Significantly, given that tumor cells typically have higher GSH levels compared to normal cells (millimolar *versus* submillimolar concentrations), the designed strategy for GSH-dependent photoactivation in this work greatly reduces the risk of nonspecific phototoxicity. Soon after, Peng and colleagues presented another organic activatable PS, termed CyI-DNBS, containing 2,4-dinitrobenzenesulfonate (DNBS) as the cage group (Fig. 4c).<sup>92</sup> CyI-DNBS can be taken up by tumor cells and selective uncaged by intracellular GSH, leading to the production of SO<sub>2</sub> for gas therapy. In addition, the reaction liberates the activated PS, CyI-OH, which can produce  $^1\text{O}_2$  for PDT with light irradiation. Furthermore, the generated SO<sub>2</sub> not only acts as a gas therapeutic agent, but its consumption of excess GSH during the production process helps break the antioxidant defense of tumor cells, thereby further increasing the level of ROS and enhancing the efficacy of PDT. Based on these advantages, CyI-DNBS exhibited excellent therapeutic effects through the combined action of PDT and gas therapy, significantly inhibiting tumor growth. Moreover, no obvious systemic toxicity was observed in normal organs, indicating good biocompatibility.

Other molecular features, such as the high concentrations of proteins and enzymes found in cancer cells, have also been utilized for activated PS for precise PDT.<sup>93-95</sup> In 2023, Miao and colleagues developed two organic pro-theranostic agents (FMP and N-FMP, Fig. 5a) with activatable fluorescence, photoacoustic imaging, and photodynamic effects in response to the biomarker fibroblast activation protein  $\alpha$  (FAP $\alpha$ ), which is overexpressed in more than 90% of human tumor cells.<sup>96</sup> Both FMP and N-FMP comprise a methylene blue motif conjugated to a FAP $\alpha$ -cleavable peptide substrate through a carbamate-based self-immolative linker.<sup>97</sup> Interestingly, because of the extended length of self-immolative linker, FMP has higher affinity and superior sensing capacity for FAP $\alpha$  than N-FMP with the short self-immolative linker. Additionally, FMP can be selectively enriched at tumor sites *via* FAP $\alpha$ -triggered peptide

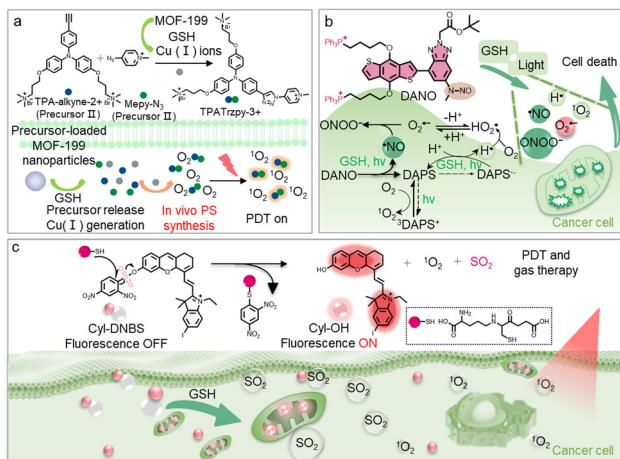
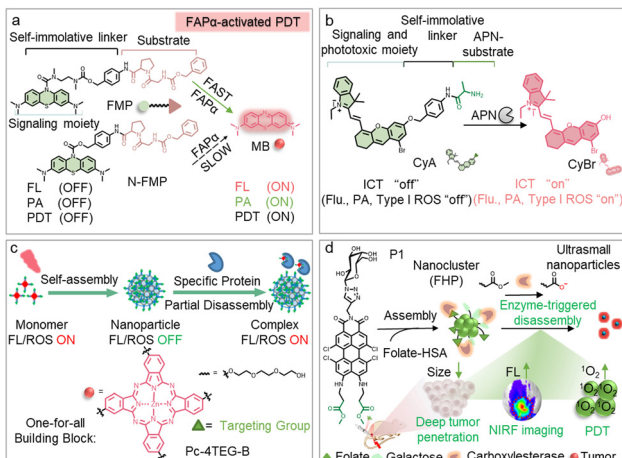


Fig. 4 (a) Cancer cell-triggered *in vivo* PS (TPATrzPy-3<sup>+</sup>) synthesis for activatable PDT. Reproduced with permission from ref. 90. Copyright, 2021, John Wiley & Sons. (b) Chemical structure of DANO and schematic of GSH-light coactivation for enhanced PDT. Reproduced with permission from ref. 91. Copyright, 2021, American Chemical Society. (c) Chemical structure of Cyl-DNBS and schematic of GSH activation for enhanced PDT and SO<sub>2</sub> gas therapy. Reproduced with permission from the ref. 92. Copyright, 2022, John Wiley & Sons.





**Fig. 5** (a) Schematic of molecular pro-theranostic agents (FMP and N-FMP) for FAP $\alpha$ -activatable PDT. Reproduced with permission from ref. 97. Copyright, 2023, John Wiley & Sons. (b) Schematic of the phototheranostic agent (CyA) for APN-activatable anti-hypoxic PDT. Reproduced with permission from ref. 98. Copyright, 2024, John Wiley & Sons. (c) Schematic of the dynamic PS (Pc-4TEG-B) assembly and partial disassembly processes, highlighting its switchable photoactivity. Reproduced with permission from ref. 104. Copyright, 2017, American Chemical Society. (d) Schematics of FHP nanocluster fabrication (assembly of P1 and folate-modified human serum albumin (Folate-HSA)), along with enzyme-induced disassembly of FHP and size reduction for activatable PDT. Reproduced with permission from ref. 105. Copyright, 2020, John Wiley & Sons.

hydrolysis, leading to the release of methylene blue molecules, thereby restoring fluorescence and photoacoustic signals for guiding PDT. Due to its effective activatable photodynamic effect on tumor cells and the induction of immunogenic cell death, complete ablation of primary tumors and distant tumors' abscopal action were observed in a preclinical model. Significantly, this work employs local activatable treatment to induce regional cell damage, which is more controllable and adjustable with minimal side effects on normal cells and tissues. Continuing their innovative work in 2024, Miao *et al.* designed another organic phototheranostic agent (CyA, Fig. 5b) with an aminopeptidase N (APN)-responsive fluorophotoacoustic signal and PDT combined with immunotherapy for effective cancer treatment.<sup>98</sup> The obtained phototheranostic agent is created by linking a hemicyanine-based type I PS (CyBr) to an APN-cleavable alanine (Ala) moiety *via* a carbamate-based linker. In the presence of APN, which is overregulated in certain malignant tumor cells,<sup>99–101</sup> CyA undergoes hydrolysis to produce the active CyBr agent with restorable intramolecular charge transfer, leading to the recovery of fluorophotoacoustic signals and photothermal activity. Upon laser illumination, CyA demonstrated effective phototoxicity, inhibiting tumor growth in mouse models. Furthermore, histological examination of major organs, including kidneys, spleen, liver, and heart, revealed no significant histopathological changes following treatment.

Controlled molecular disassembly has been proven to be an effective approach for developing smart nanoassembly-based therapeutic agents.<sup>38,102,103</sup> By incorporating stimulus-responsive

segments into the building blocks, nanostructure assemblies can be triggered by specific stimuli, enabling controlled performance for diagnosis and treatment. In 2017, Li *et al.* synthesized nanostructure phthalocyanine assemblies (NanoPcTB) using self-assembled Pc-4TEG-B monomers as a versatile PS (Fig. 5c).<sup>104</sup> Pc-4TEG-B was created by attaching four biotins as targeting groups to the zinc(II) phthalocyanine core. Due to the unique non-covalent interactions between the targeting groups and phthalocyanine, these spherical nanostructure assemblies exhibit targeted protein-driven partial disassembly. Consequently, NanoPcTB serves as an effective PS for cancer-specific induced-fluorescence imaging and therapeutic applications. Following systemic injection, NanoPcTB accumulated at tumor sites in a preclinical model, and laser irradiation significantly inhibited tumor growth. Subsequently, Cai and co-workers developed a perylene monoamide-based nanocluster capable of enzymatic decomposition, showcasing deep tumor penetration ability for activatable photodynamic treatment.<sup>105</sup> As shown in Fig. 5d, the precursor P1 was synthesized by modifying the tetrachloroperylene monoimide core with galactose, which serves as both the hydrophilic group and the tumor-targeting ligand, and  $\beta$ -alanine methyl ester, which functions as both the electron donor and the carboxylesterase substrate. The resulting amphiphilic P1 can self-assemble with folate-modified human serum albumins to form nanoclusters (FHP) with a size of approximately 100 nm. Once P1 is selectively hydrolyzed by carboxylesterase at tumor sites, FHP decomposes into small nanoparticles (about 10 nm), facilitating deep tumor penetration. In addition, the carboxylesterase-induced decomposition of FHP enhances fluorescence by approximately 8-fold and photodynamic activity by approximately 4-fold, improving diagnostic accuracy and treatment effectiveness. As a result, following a single intravenous administration and illumination, FHP realized significant tumor suppression (97%) in mouse models with minimal side effects.

## 2.2. Dual activatable PSs

To enhance the precision of cancer treatment in complex biological environments, smart phototheranostic agents that respond to multiple simultaneous stimuli are highly desirable. Such agents can provide robust and highly specific activation, thereby improving treatment accuracy and overall safety (Fig. 6a).<sup>62,93,106,107</sup> Yang and co-workers developed a “dual lock-and-key” supramolecular nanotheranostic agent (named as BIBCl-PAE NPs, Fig. 6b) to provide enhanced specificity in cancer treatment.<sup>108</sup> In this system, BIBCl-PAE NPs are developed through encapsulating a rationally designed GSH-triggered (first lock-and-key) PS (BIBCl) in a pH-activatable (second lock-and-key) diblock copolymer. In blood and normal tissues with low GSH levels and neutral pH, the amphiphilic polymer and the hydrophobicity of BIBCl are significant as “double locks”, maintaining the PS in a highly aggregated state. This aggregation leads to the aggregation-caused quenching (ACQ) effect, preventing the generation of  $^1\text{O}_2$ . However, in the tumor microenvironment, characterized by the high GSH concentrations and low pH, the “dual keys” of GSH and pH unlock the ACQ state of PS, promoting ROS generation to



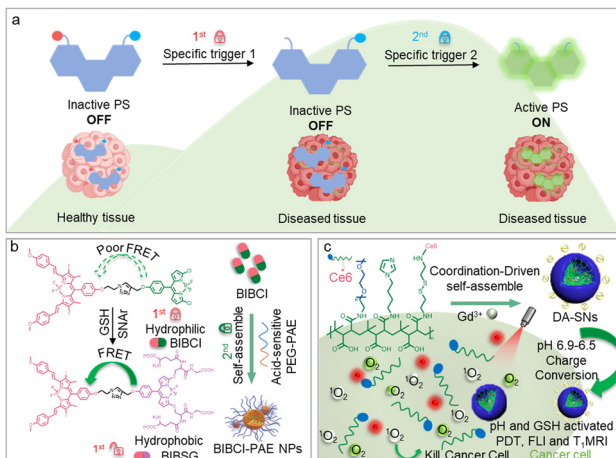


Fig. 6 (a) Schematic of the working principle of dual-activatable PS for enhanced safety of PDT. (b) Schematics of the fabrication of BIBCI-PAE NPs and the “dual lock-and-key” mechanism in the tumor microenvironment for activated and enhanced generation of  $^1\text{O}_2$ . Reproduced with permission from ref. 108. Copyright, 2020, Royal Society of Chemistry. (c) Schematic of the fabrication of DA-SNs through coordination-driven self-assembly and their dual activation for improving the specificity of PDT. Reproduced with permission from ref. 109. Copyright, 2020, Elsevier.

selectively damage cancer cells under light irradiation. These features enable the smart phototheranostic agent to exhibit exceptional specificity and improved phototherapeutic response both *in vitro* and *in vivo*, while minimizing side effects. In the same year, Fu and his colleagues prepared a redox and pH dual-responsive self-assembled phototheranostic agent, termed DA-SNs (Fig. 6c), through the self-assembly of gadolinium ions ( $\text{Gd}^{3+}$ ) and a Ce6 disulfide-connected pH-activatable polymer ligand.<sup>109</sup> Interestingly, the surface charge of DA-SNs can transition from negative to positive in the slightly acidic extracellular environment of tumors, enhancing cellular uptake. Once inside tumor cells, fluorescence and photodynamic effects can be activated under intracellular conditions characterized by high GSH levels and low pH. Consequently, DA-SNs efficiently suppress tumor growth with minimal side effects.

In a more recent study, Chen *et al.* fabricated a complex nanosystem named JSK@PEG-IR820 to deliver nitric oxide (NO) and achieve type I PDT (Fig. 7a).<sup>110</sup> JSK@PEG-IR820 consisted of three key components: a photo-triggered phototheranostic agent (IR820), a pH-activatable moiety (diisopropyl), and a NO precursor ( $\text{O}_2$ -(2,4-dinitrophenyl)-1-[(4-ethoxycarbonyl)piperazin-1-yl]diazen-1-ium-1,2-diolate, known as JSK). The diisopropyl group in this system serves a dual purpose: acting as a pH-sensitive moiety for the breakdown of JSK@PEG-IR820 to release JSK and enhancing intermolecular electron transfer to IR820, thereby prompting efficient type I ROS production. Simultaneously, the release of JSK leads to GSH consumption, leading to the generation of NO. This dual-action strategy significantly enhances the phototherapeutic efficacy, ultimately realizing complete tumor growth suppression. Specifically, no adverse effects were detected in normal tissues, emphasizing the high biosafety profile of this nanotheranostic agent.

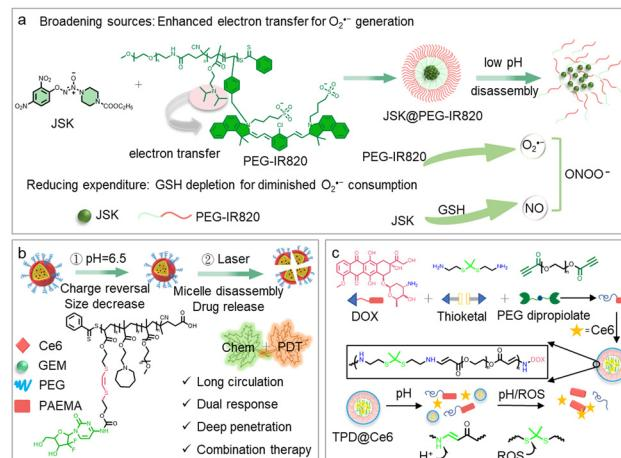


Fig. 7 (a) Schematic of the synthesis of the nanotheranostic agent (JSK@PEG-IR820) for pH and GSH coactivation to enhance PDT and gas therapy with minimal side effects. Reproduced with permission from ref. 110. Copyright, 2024, American Chemical Society. (b) Schematic of a phototheranostic agent for combined chemotherapy and PDT under dual activation by pH and laser. Reproduced with permission from ref. 114. Copyright, 2020, Royal Society of Chemistry. (c) Schematic of the synthesis of a nanotheranostic agent (TPD@Ce6) for pH and ROS coactivation for enhanced PDT and chemotherapy with high safety. Reproduced with permission from ref. 115. Copyright, 2021, American Chemical Society.

In recent decades, polymer-drug conjugates have garnered significant attention as responsive phototheranostic agents for activatable treatment due to their enhanced hydrophilicity, improved pharmacokinetics, and superior drug utilization compared to traditional hydrophobic PSs.<sup>111–113</sup> For instance, Chen and colleagues presented a multifunctional drug carrier nanosystem based on pH and  $^1\text{O}_2$  dual-activatable gemtuzumab (GEM) prodrug polymer micelles co-encapsulated with Ce6 to improve the therapeutic efficacy by combining PDT and chemotherapy.<sup>114</sup> As demonstrated in Fig. 7b, GEM was covalently attached to the polymer *via* a  $^1\text{O}_2$  sensitive linker, reducing GEM leakage in normal tissues to minimize side effects. Simultaneously, Ce6-loaded prodrug micelles displayed excellent tumor enrichment capacity. Upon reaching the tumor sites, the acidic tumor environment triggered the release of Ce6, which could sustainably generate  $^1\text{O}_2$ , breaking the  $^1\text{O}_2$ -sensitive linker and facilitating the robust release of GEM to realize an effective treatment with negligible side effects. Subsequently, Zhang *et al.* developed another pH and ROS dual-activatable polymer-drug conjugate (referred to as TPD, Fig. 7c) using the antitumor drug doxorubicin containing an amine, a thioketal molecule with amino groups (TKL), and water-soluble poly(ethylene glycol) propiolate.<sup>115</sup> In addition, they utilized this amphiphilic prodrug as a carrier to effectively load the PS Ce6 for PDT. Owing to the ROS sensitivity of the thioketal bond and the pH responsiveness of the alkylene-amine bond in TPD, TPD@Ce6 was designed to cleave in a tumor microenvironment, releasing Ce6 and doxorubicin for targeted combination therapy of PDT and chemotherapy.

Enzymes are widely distributed in various normal tissues throughout the body, with approximately 580 types of hydrolytic

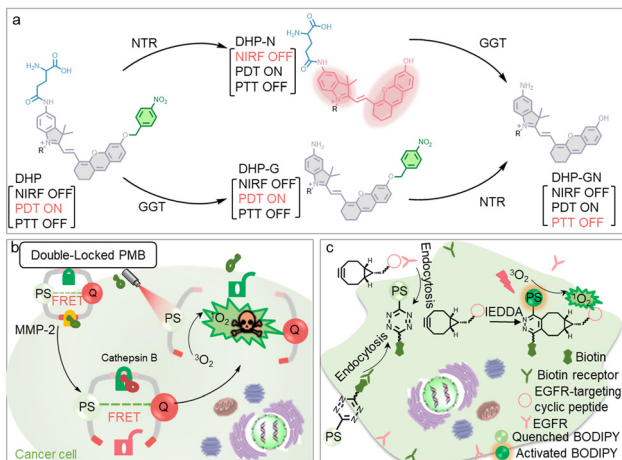


Fig. 8 (a) Schematic of the molecular mechanism of self-regulated PDT-PTT by a phototheranostic agent in the presence of GGT and NTR. Reproduced with permission from ref. 118. Copyright, 2022, John Wiley & Sons. (b) Schematic of a molecular pro-theranostic agent for dual enzyme-activated PDT to improve treatment safety. Reproduced with permission from ref. 120. Copyright, 2023, American Chemical Society. (c) Schematic of the bioorthogonal activation of PS via inverse electron-demand Diels–Alder reaction. Reproduced with permission from ref. 121. Copyright, 2023, John Wiley & Sons.

proteases present in the human body.<sup>116</sup> Numerous studies have demonstrated abnormal expression of enzyme concentrations in various pathological processes.<sup>117</sup> To enhance the targeting specificity of enzyme-activated single-lock PSs, researchers have developed enzyme-responsive dual-lock PSs to improve the biosafety of PDT. For example, Wei and co-workers introduced a dual-locked activatable phototheranostic agent, termed DHP, for *in vivo* NIR imaging and adaptive PTT-PDT cancer treatment (Fig. 8a).<sup>118</sup> This agent comprises a dual-responsive hemicyanine (DHCy) dye surrounded by two enzyme-triggered groups and a poly(ethylene-glycol) (PEG) chain to enhance biocompatibility. In this system, the hypoxia-related enzyme nitroreductase (NTR) and the cancer-overexpressed enzyme  $\gamma$ -glutamyl transferase (GGT) were selected as biomarkers to induce NIR fluorescence signals and adjust treatment modalities. Initially, DHP does not emit fluorescence due to the hindrance of ICT caused by blocking the electron-donating hydroxyl group with an NTR-cleavable substrate. Upon systemic injection and accumulation at the tumor site, this phototheranostic agent undergoes structural transformation through two enzymatic-cleavage pathways. In the vicinity of the tumor, the GGT-reactive group is cleaved at the amide moiety by efficient GGT, producing non-fluorescent DHP-G with active PDT. Thereafter, within the hypoxic core of the tumor where NTR is highly expressed, the NTR-responsive fragment of DHP-G undergoes 1,6-self-elimination to convert the nitro group to an amino group, resulting in non-fluorescent DHP-GN with active PTT instead of PDT. This autonomously regulated PTT-PDT treatment mode achieves complete tumor ablation with minimal side effects. Moreover, if the NTR-activatable fraction is cleaved before the GGT-activatable fraction, highly fluorescent DHP-N is obtained,

enabling real-time NIR fluorescence imaging. This phototheranostic agent exemplifies a promising molecular design strategy for precise cancer phototherapy.

In a separate study, Dennis and colleagues presented a dual stimuli-activated PS in which two or three GSH-activatable DNBS-modified zinc(II) phthalocyanine moieties are linked through cathepsin B-cleavable Gly-Phe-Leu-Gly peptide linkers.<sup>119</sup> These polymeric phthalocyanines were fully quenched initially due to the photoinduced electron transfer to the DNBS fragment and self-quenching of the phthalocyanine units. However, upon exposure to cathepsin B and GSH or upon internalization into cancer cells (including HepG2 human hepatocarcinoma cells and A549 human lung carcinoma cells), these phototheranostic agents could be selectively activated by releasing free phthalocyanine moieties. Specifically, leveraging this activatable feature, the photocytotoxicity of these phototheranostic agents relied on the intracellular levels of cathepsin B and GSH. These findings illustrated the potential of these conjugates as smart PSs for precise cancer treatment. Building on their innovative work, in 2023, Dennis's group developed a novel photodynamic molecular beacon (PMB, Fig. 8b), which is exclusively activated in the presence of both cathepsin B and matrix metalloproteinase-2 (MMP-2).<sup>120</sup> Cathepsin B is a lysosomal cysteine protease overexpressed in various tumors, while MMP-2 is an extracellular membrane-bound enzyme upregulated in most malignancies, serving as a crucial biomarker for cancer diagnosis and prognosis. This “double-responsive” PMB is extensively quenched in its basal state and remains inactive even in the presence of one of these biomarkers; activation occurs only when both enzymes are present. This unique property allows the PMB to function as an enzyme-based logic gate and serve as targeted PS for precise PDT against cancer. Consequently, the PMB effectively suppressed tumor growth in A549-tumor-bearing nude mice under laser irradiation. Furthermore, while the light excitation of the other “always-ON” PSs led to severe skin damage in the mice, the double-activatable PMB caused minimal cellular damage to the skin tissues even under laser irradiation, indicating favourable biosafety.

In the same year, Jacky *et al.* presented an advanced dual receptor-mediated biorthogonal responsive strategy to enhance the tumor specificity of the photodynamic effect.<sup>121</sup> As shown in Fig. 8c, this system comprises a biotinylated tetrazine-substituted BODIPY and a cyclic epidermal growth factor receptor (EGFR)-targeting peptide linked with a bicyclic[6.1.0]non-4-yne dienophile. The tetrazine moiety was included to efficiently quench the fluorescence emission and ROS generation of the BODIPY core. These two components selectively bind to the EGFR and biotin receptors, which are overexpressed on the membrane of cancer cells. Specifically, only cells that overexpress both biomarkers can internalize the compounds, leading to a rapid bioorthogonal inverse electron-demand Diels–Alder reaction that eliminates the tetrazine quenching fragment by forming the corresponding cycloadduct. As a result, the BODIPY core is activated, restoring fluorescence emission and ROS production. Through experiments by using various cell lines with different biotin receptor and EGFR expression levels, it has demonstrated that significant ROS generation and cytotoxicity activation occur exclusively in A549 cells



positive for both biotin receptors and EGFR. Therefore, compared to “always-ON” photodynamic systems, this method allows precise control of photodynamic activity in a highly specific manner, significantly enhancing the treatment specificity and biosafety.

### 2.3. Reversible PSs

The development of reversible PSs that can selectively modulate photodynamic activity in response to specific stimuli is crucial for therapeutic and diagnostic applications. Achieving reversibly switchable photodynamic activity in response to pathological stimuli, such as pH changes, hypoxia, or exposure to enzymes, is essential for advancing PDT. When the PS is translocated or metabolized away from the pathological area, the switchable photodynamic activity can be turned off to deactivate the PDT action. This capability helps address common limitations of the current PDT paradigm, including inevitable damage to normal tissues and persistent skin photosensitivity (Fig. 9a).

In the field of enhanced *in vivo* precise PDT, pH-responsive phototheranostic agents offer observably advantages, particularly in situations where pH fluctuations occur due to physiological and pathological conditions, creating opportunities for the development of reversible PSs. In 2019, Hu *et al.* proposed an approach to achieve reversible switching of ISC in a novel PS that exhibits pH-triggered conjugated backbone distortion (PE5, Fig. 9b).<sup>122</sup> The organic conjugated obtained demonstrated significantly improved ISC efficiency in a slightly acidic environment, increasing from nearly 0% to 90% by enhancing the degree of molecular distortion. This provides an innovative mechanism to facilitate ISC and achieve robust photodynamic effects only under pathological stimuli. Specifically, the ISC process can be deactivated to halt the photodynamic action and

further enhance treatment safety, when the phototheranostic agent is eliminated or metabolized from the pathological tissues.

Soon after, Tang and colleagues introduced another reversible pH-responsive phototheranostic agent (referred to as DTTVBI) with AIE properties for NIR-II fluorescence imaging-guided synergistic PDT and PTT.<sup>123</sup> As displayed in Fig. 9c, DTTVBI was designed by incorporating benzo[*c,d*]indolium as the electron-accepting moiety, utilizing donor engineering, where the C=N double bond acts as the pH-activatable unit. Owing to strong donor-acceptor interactions, small singlet-triplet energy gaps, and abundant molecular rotors, DTTVBI exhibits NIR-II AIE characteristics, high ROS generation efficiency, and remarkable photothermal conversion performance. Specifically, upon cyclic pH adjustments between 4.0 and 10.0 in the BR buffer, DTTVBI demonstrated a satisfactory reversibility attributed to the cleavage and restoration of the C=N double bond, resulting in visible color changes from dark green to light yellow. Moreover, both *in vitro* and *in vivo* experiments demonstrated that DTTVBI exhibited notable pH reversibility, NIR-II fluorescence tumor imaging ability, and exceptional antitumor efficacy attributed to the combination effect of PDT and PTT in a preclinical model. Additionally, no histological differences were observed in the hematoxylin and eosin staining images of major organs, indicating minimal systemic toxicity of DTTVBI. Another NIR-II PS, RBT-PH-1 NPs ( $pK_a = 6.76$ ), designed for reversible pH-triggered imaging and treatment, was fabricated by Wang and co-workers.<sup>124</sup> By introducing heavy halogen atoms, the spin-orbit coupling is improved and the relative energy gap between the singlet excited state and triplet excited states is decreased, thus improving ISC efficiency and leading to higher ROS generation efficiency. Within the acidic tumor microenvironment, a fraction of the helical lactam rings of RBT-PH-1 underwent opening to form RBTH<sup>+</sup>, leading to the recovery of the fluorescence signal and ROS generation ability upon laser irradiation. This mechanism facilitated precise tumor imaging guidance and effective tumor growth suppression with high biosafety standards.

In 2023, Liu and colleagues proposed a design for an on-demand switchable phototheranostic agent to minimize side effects before and after treatment.<sup>125</sup> The photodynamic activity is based on a reversible, activatable mechanism, allowing the phototheranostic agent to remain non-toxic in normal tissues before, during, and after treatment, only converting into a phototoxic form in the hypoxic tumor microenvironment. As a proof-of-concept, a hypoxia-normoxia cycling responsive PS (termed TPFN-AzoCF<sub>3</sub>, Fig. 9d) containing an arylazo group was designed and synthesized. In this system, the arylazo group acts as an effective cyclic responsive trigger that can be reversibly converted into a hydrazine group depending on normoxia-hypoxia conditions. Under normoxic environments, its rapid *E*-*Z* isomerization with light illumination effectively quenches the excited-state energy of the phototheranostic agent, a process that is disabled only under hypoxic conditions, where the aryl azo group is converted into a hydrazine group, thereby activating the PS and

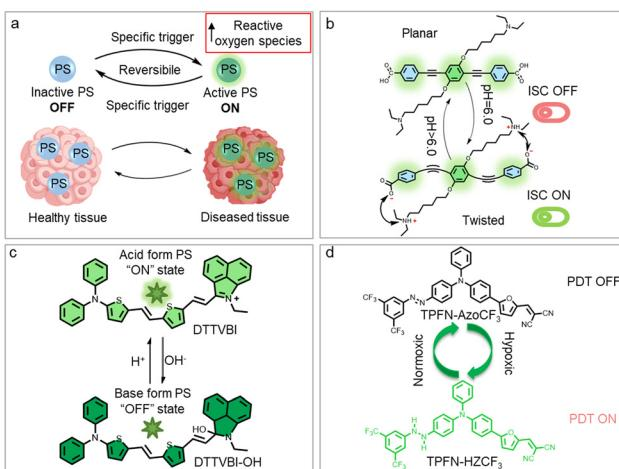


Fig. 9 (a) Schematic of the working principle of a reversible PS to enhance PDT safety. (b) Schematic of the reversible switching of ISC and its potential in smart PDT. Reproduced with permission from ref. 122. Copyright, 2019, John Wiley & Sons. (c) Schematic of PS (DTTVBI) as a tumor pH-reversible theranostic platform for precise PDT. Reproduced with permission from ref. 123. Copyright, 2023, American Chemical Society. (d) Schematic of the working principle of a hypoxia-normoxia reversible PS for enhancing PDT safety. Reproduced with permission from ref. 125. Copyright, 2023, John Wiley & Sons.



enabling ROS generation. Specifically, the hypoxia-dependent reversibility and tumor suppression efficiency of TPFN-AzoCF3 were monitored in mouse models, which demonstrated its significant antitumor action with safe pre- and post-treatment for PDT.

More recently, Yang and co-workers presented a BODIPY-based PS (BODIPY 1) designed for activation in the tumor microenvironment.<sup>126</sup> This derivative of BODIPY was chemically modified with *p*-nitrophenol as leaving groups at the 3,5-positions, enabling it to act as a molecular chameleon with cascade switching capacity. This design allows for precise control of PS delivery, thereby enhancing the specificity of PDT. To prevent BODIPY 1 from generating ROS in blood and normal tissues, it was encapsulated in a pH-switchable surfactant to create BODIPY 1a with a PEGylated surface. Encouragingly, once localized at the tumor site, BODIPY 1a was activated within cancer cells due to the high concentration of GSH and the weakly acidic environment, resulting in the formation of the hydrophilic product BODIPY 2. Upon exposure to light, BODIPY 2 can generate ROS, which induce cancer cell death through the pyroptosis pathway. As a result, mice treated with BODIPY 1 followed by light irradiation displayed significant tumor inhibition, with a regression rate of 83.2% after a 20-day treatment period. Notably, following PDT completion, BODIPY 2 underwent gradual degradation to produce the non-phototoxic product BODIPY 3. This transformation was facilitated by hydrolysis and intramolecular rearrangement reactions catalyzed by the overexpressed gamma glutamyltranspeptidase, thereby enhancing biosafety both pre- and post-treatment.

### 3. Biosafety enhancement of PDT by degradable PSs

Recently, phototheranostic agents that degrade after PDT have emerged to improve safety post-treatment. The decomposed PS loses its ability to generate ROS, thereby reducing side effects following PDT (Fig. 10a). Degradable PSs show significant promise in addressing safety concerns post-PDT. Currently, most intentionally designed degradable phototheranostic agents decompose *via* self-generated ROS.<sup>127</sup> Photostability is one of important parameters for assessing the potential of PSs for PDT, which refers to the stability of PSs upon light irradiation. However, photostability is more like a double-edged sword. On the one hand, the over-stable feature may impact the PS metabolism after PDT and induce the potential toxicity of drug accumulation. On the other hand, the over-rapid photodegradation of PS during the process of PDT may influence the therapeutic efficacy. Therefore, exploring the appropriate spot of photodegradation, in which PS demonstrates effective photodynamic effect in therapy and could be degraded after treatment, would decrease the side effects and further enhance the biosafety of PDT. In 2020, Zhang and co-workers introduced a supramolecular strategy to regulate the photoactivity and photodegradation of PS, developing a BODIPY-based

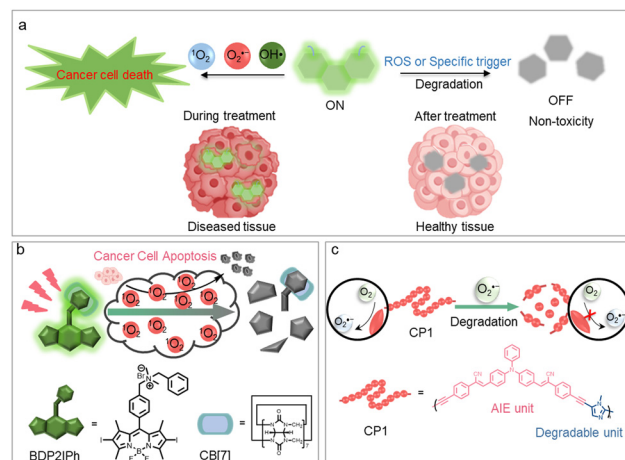


Fig. 10 (a) Schematic of the working principle of a degradable PS for improved PDT safety. (b) Representation of a self-degradable PS (BDP2IPh) for minimizing PDT side effects. Reproduced with permission from ref. 128. Copyright, 2021, John Wiley & Sons. (c) Representation of a self-degradable PS (CP1) for enhanced PDT safety. Reproduced with permission from ref. 129. Copyright, 2022, John Wiley & Sons.

cationic supramolecular PS (named BDP2IPh, Fig. 10b).<sup>128</sup> Cucurbit[n]urils (CB[n]) are a class of highly symmetric macrocyclic compounds composed of glycoluril units. Because of the electrostatic interactions of the carbonyl groups on both sides of CB[n], they can be employed to rationally regulate the photoactivity of guest molecules such as organic PSs. Specifically, after BDP2IPh binding with CB[7], the resulting supramolecular PS BDP2IPh-CB[7] exhibited a significantly prolonged triplet-state lifetime, thereby demonstrating enhanced ROS generation capability. The results of *in vitro* experimental confirmed that BDP2IPh-CB[7] can effectively kill tumor cells under light irradiation. Notably, the incorporation of CB[7] can also provide BDP2IPh with excellent self-degradation features. During PDT treatment, the ROS photo-induced by BDP2IPh-CB[7] not only eradicates tumor cells but also facilitates PS degradation. Post-treatment, most PS molecules lose their photoactivity, converting into low-toxicity micro-molecules. The results of *in vitro* experiments exhibited that the irradiation-treated BDP2IPh-CB[7] demonstrated minimal cytotoxicity even under light irradiation. In this way, potential side effects post-PDT are minimized, enhancing the overall safety of PDT.

In 2022, Huang *et al.* developed a self-degradable PS (CP-NPs) based on a conjugated polymer consisting of AIE and imidazole moieties.<sup>129</sup> As shown in Fig. 10c, owing to the effective conjugated backbone and unique AIE nature, the resulting polymer-based PS efficiently produces O<sub>2</sub><sup>•-</sup> through type I photoreaction under light irradiation, suitable for hypoxic tumor treatment. The O<sub>2</sub><sup>•-</sup> generated by CP-NPs can further trigger the self-degradation of the polymer to yield non-toxic small molecules. This process not only addresses potential phototoxicity issues of residual phototheranostic agents but also accelerates the clearance of the conjugated polymers from the body to minimize potential biotoxicity from drug accumulation. Both *in vitro* and *in vivo* experiments



proved that CP-NPs effectively suppress tumor growth under light irradiation and reduce potential side effects. In 2023, Huang and colleagues continuing their innovative efforts by preparing another self-degradable PS based on a conjugated polymer to load the immune adjuvant, achieving synergistic photodynamic and immunotherapy while simultaneously minimizing the potential biotoxicity from drug accumulation.<sup>130</sup>

In the same year, a degradable PS (named SQO, Fig. 11a) was successfully developed based on the dicyano-modified squaraine by Li *et al.*<sup>131</sup> To further enhance the ROS generation efficiency, they subsequently replaced "S" with "Se" to construct a symmetric photosensitizer (SQSe). Encouragingly, SQSe demonstrated excellent capability to generate various ROS upon light exposure (including  $^1\text{O}_2$ ,  $\text{O}_2^{\cdot-}$ , and  $\text{OH}^{\cdot}$ ) compared with that of SQO because the heavy atom effect enhances the ISC process, enabling more energy to be transferred to the triplet state, ultimately promoting the generation of ROS. Specifically,  $^1\text{O}_2$  and  $\text{O}_2^{\cdot-}$  can suppress the tumor growth for PDT, while  $\text{OH}^{\cdot}$  oxidize the PS itself for rapid photodegradation. After photodegradation for 10 min, the *in vitro* photocytotoxicity of SQSe was significantly decreased due to the decreased photosensitization efficiency. Furthermore, the degradation byproducts were subsequently eliminated from the body *via* urine to further enhance biosafety. These diverse degradation mechanisms ensure rapid loss of photoactivity by the PS, thereby minimizing the potential side effects of residual PSs post-PDT. Analysis of blood biochemistry analysis in a preclinical model demonstrated that SQSe offers a significant safety advantage over the commercial PS Ce6 in the post-operative period.

Anthracene, as a  $\pi$ -conjugated structure, can be oxidized by  $^1\text{O}_2$  to form a  $\pi$ -cleaved endoperoxide, which subsequently decomposes into anthraquinone and oxanthrone.<sup>132</sup> This characteristic makes the anthracene moiety an ideal candidate for constructing degradable PSs with well-defined decomposition components to further understand the pharmacokinetics of degradable PSs and improve post-PDT safety. Based on this rationale, Gao and co-workers developed an efficient and degradable phototheranostic agent, termed TPA-An-DPP, by integrating an anthracene bridge into a donor–acceptor structure (Fig. 11b).<sup>133</sup> Notably, the steric hindrance of the anthracene bridge can modulate the orbital distribution, thereby enhancing the  $^1\text{O}_2$  generation capacity and therapeutic effectiveness of the PS. In addition, the self-generated  $^1\text{O}_2$  can oxidize the anthracene bridge into endoperoxide- and anthraquinone-derived units, disrupting the  $\pi$ -conjugation and consequently halting the  $^1\text{O}_2$  generation to reduce post-phototoxicity following treatment. Consequently, the resulting PS, TPA-An-DPP, achieves a balance between therapeutic efficacy and self-quenching, ensuring both effective PDT treatment and post-treatment safety. In the same year, Li and colleagues utilized a molecular surgery method to fabricate a self-degradable nanostructure phototheranostic agent (NanoPcDA2) through the self-assembly of a phthalocyanine derivative (PcDA2).<sup>134</sup> As shown in Fig. 11c, NanoPcDA2 demonstrated a significant heat generation ability to impede tumor growth under light exposure. As a result, in a mice tumor model, 92% tumor growth was inhibited at a NanoPcDA2 dose of  $0.8 \text{ nmol g}^{-1}$  and a low light dose of  $300 \text{ J cm}^{-2}$ . Furthermore, NanoPcDA2 can be decomposed into three small, well-defined fragments through self-generated  $^1\text{O}_2$ , resulting in the loss of its photoactivity after treatment. More importantly, minimal cytotoxicity was observed for the photodegradation products of NanoPcDA2. This approach not only addresses potential phototoxicity concerns from residual phototheranostic agents but also accelerates the metabolism of the phototheranostic agent to mitigate potential biotoxicity arising from drug accumulation.

PSs that degrade *via* self-generated ROS under light irradiation exhibit high spatial and temporal precision, and are easily controllable in real time. In addition, the treatment process can be achieved simultaneously with the degradation process. However, this approach may require the accumulation of ROS and is limited by poor penetration depth of light. In addition to decomposition by self-generated ROS, some intentionally designed decomposable PSs can also be induced to decompose after PDT by small biological molecules, such as  $\text{H}_2\text{O}_2$  and NTR. PSs that degrade by endogenous biomolecules have high specificity. In 2020, Lee *et al.* developed a degradable graphene oxide (GO) nanoplatform (GO-He-G4-M@DOX) by applying catalytic DNA, realizing efficient *in vivo* self-degradation and controlled antitumor therapeutic effects.<sup>135</sup> Once the GO-He-G4-M@DOX was internalized *via* mucin1 aptamer-mediated endocytosis, a photo-switch induced the liberation of doxorubicin from the DNA. Subsequently, the single-stranded G-quadruplex sequences on the GO surface folded into quadruplex structures and bound with hemin to form DNAzymes,

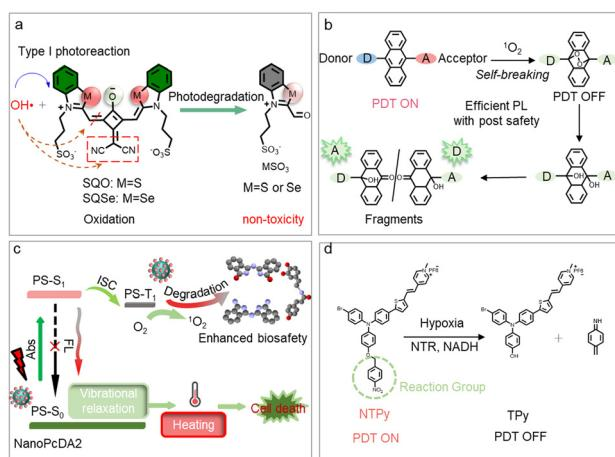


Fig. 11 (a) Schematic of the phototheranostic agent (SQSe) with multiple degradation modes for postoperatively safe PDT. Reproduced with permission from ref. 131. Copyright, 2023, Elsevier. (b) Chemical structure of an anthracene-bridged donor–acceptor PS and its self-degradation mechanism, where generated  $^1\text{O}_2$  oxidizes anthracene into endoperoxide- and anthrone-derived fragments, disrupting photosensitizing activity. Reproduced with permission from ref. 133. Copyright, 2023, American Chemical Society. (c) Schematic of the mechanism of heat generation and photo-degradation of PS post-treatment to reduce phototoxicity. Reproduced with permission from ref. 134. Copyright, 2023, Elsevier. (d) Representation of degradable PS (NTPy) for reducing PDT-related side effects. Reproduced with permission from ref. 136. Copyright, 2022, Elsevier.



exhibiting peroxidase-like activity. Owing to the high content of  $H_2O_2$  in the tumor microenvironment, the catalytic GO nano-platforms could generate a large amount of the strong oxidizing agent hypochlorous acid, which promoted GO decomposition into small components for efficient elimination from the body.

In a recent study, Shi and co-workers synthesized a smart AIE luminogen (NTPy) containing 4-nitrobenzyl as the recognition unit for NTR (Fig. 11d).<sup>136</sup> NTPy demonstrated strong fluorescence emission and high ROS generation efficacy due to its AIE properties. Under hypoxic conditions, NTPy underwent decomposition into distinct fragments through the reduction induced by NTR. The resulting degraded products exhibited reduced photodynamic activity but excellent biocompatibility. Effective PDT with minimal side effects were realized by precise control of the dosage and treatment duration of NTPy and PDT, respectively. This research introduces a novel strategy to improve the biosafety of residual PS post-PDT while maintaining treatment efficacy.

## 4. Renal-clearable PSs for enhanced biosafety in PDT

The FDA mandates that all injectable phototheranostic agents must be completely cleared from the body within a reasonable time frame.<sup>137</sup> Therefore, ensuring the renal clearance of phototheranostic agents is crucial for their future clinical success. Phototheranostic agents that are renal-clearable are eliminated through the renal metabolic system showing potential in reducing systemic toxicity by avoiding non-specific accumulation in normal tissues or organs.<sup>138</sup> In addition, renal excretion, with minimal intracellular metabolism compared to the hepatobiliary system, can further decrease the retention and toxicity of these agents.<sup>139</sup> Therefore, renal clearance is deemed the optimal elimination route. Nanotechnology is a rapidly advancing field, with many nanoparticles under scrutiny as phototheranostic agents for clinical applications.<sup>140–142</sup> Nanoparticles of larger size may be sequestered by the reticuloendothelial system, leading to systemic accumulation and potential long-term toxicity.<sup>143,144</sup> In contrast, spherical nanoparticles with a hydrodynamic diameter smaller than 6 nm easily traverse the glomerular capillary wall due to their unique structure (Fig. 12a).<sup>145,146</sup> To maximize the treatment efficacy and biosafety, the development of small-sized nanostructured PSs with rapid renal clearance capability is highly desirable.

PEGylation is a commonly used surface modification technique for creating renal nanoparticles. In 2017, Yang and colleagues synthesized ultrasmall black phosphorus quantum dots (BPQDs, Fig. 12b) and investigated their potential as a phototheranostic agent for PDT.<sup>147</sup> Remarkably, when exposed to light, the highly stable BPQDs effectively generated ROS. Both the results of *in vitro* and *in vivo* experiments demonstrated the BPQDs' significant antitumor efficacy through photodynamic action. Owing to their minute particle size (5.4 nm), the BPQDs can be rapidly obliterated from the body through renal clearance, reducing potential side effects. No significant organ damage or inflammatory lesions were monitored in

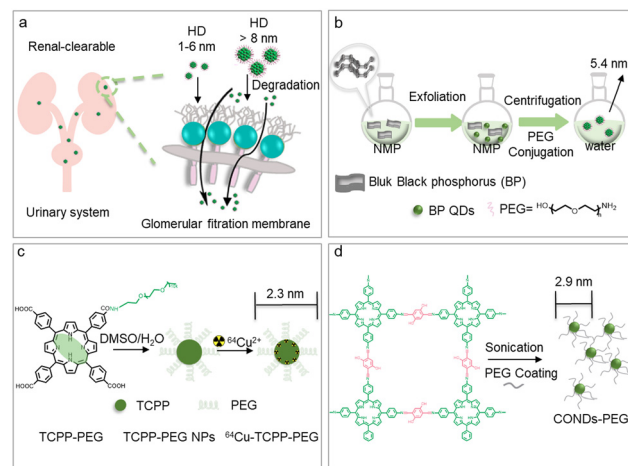


Fig. 12 (a) Schematic of the working principle of a renal-clearable PS for enhancing PDT safety. Schematics of the syntheses of ultrasmall renal-clearable nanotheranostic agents: (b) BPQDs, (c)  $^{64}\text{Cu}$ -TCPP-PEG, and (d) CONDs-PEG. Reproduced with permissions from ref. 147. Copyright, 2018, John Wiley & Sons; ref. 150. Copyright, 2017, John Wiley & Sons; and ref. 152. Copyright, 2019, American Chemical Society, respectively.

major organs, such as the kidneys, lungs, spleen, liver, and heart of mice 16-days after the treatments, demonstrating the long-term biosafety of BPQD-mediated PDT. Overall, the BPQDs serve as a potent PS for effective and safe PDT.

Porphyrin and its derivatives have been extensively developed as PSs for tumor diagnosis and treatment due to their enhanced affinity for tumor cells.<sup>106,148,149</sup> However, the hydrophobic nature of most porphyrins has hindered their clinical applications. In 2017, Cheng *et al.* added PEG to tetra(4-carboxyphenyl)-porphyrin (TCPP) to improve its water solubility and increase the molecular volume, thereby enhancing its tumor localization.<sup>150</sup> They attached PEG molecules of varying weights (2, 5, 10, and 30 KDa) to TCPP and evaluated the renal clearance and tumor uptake behavior of the resulting TCPP-PEG nanoparticles. The study revealed that TCPP-PEG nanoparticles with lower molecular weights are more readily cleared by the kidneys, while larger ones exhibit increased tumor uptake due to the EPR effect. Notably, the TCPP-PEG<sub>10K</sub> nanoparticles (Fig. 12c), with a hydrodynamic size of approximately 10 nm, emerged as a promising candidate for balancing tumor uptake and renal clearance. Both *in vitro* and *in vivo* investigations demonstrated the remarkable antitumor efficacy of TCPP-PEG<sub>10K</sub> nanoparticles. This research introduces a straightforward method for fabricating biocompatible and multifunctional phototheranostic agents with renal clearance properties. Building on this work, in 2020, Cheng and co-workers utilized a similar strategy to produce the ultrasmall pyropheophorbide-a (Pa)-PEG conjugate nanodots (2 nm) with renal clearance capabilities.<sup>151</sup> *In vivo* studies confirmed the ability of Pa-PEG nanodots to effectively suppress tumors following PDT treatment. Importantly, the nanodots were rapidly metabolized from the body through renal excretion owing to their extremely small particle size, with no observed long-term toxicity in mouse models.



To enhance the ROS generation efficacy, the porphyrin-based covalent organic framework (COF) nanodots were synthesized using a simple liquid exfoliation method by Zhang and colleagues (Fig. 12d).<sup>152</sup> The well-separated porphyrin molecules within the COF nanodots significantly improved the light-induced ROS generation capacity, leading to notable PDT efficacy and effective tumor enrichment. Furthermore, to improve the solubility and biocompatibility of the COFs, PEG was employed to coat the COFs' surface through hydrophobic interactions. The average size of the resulting PEG-coated porphyrin-based COFs (COF nanodots-PEG) observed in transmission electron microscopy images was approximately 3.5 nm. Owing to their ultrasmall particle size, the COF nanodot-PEG can be eliminated from the body through renal clearance without appreciable *in vivo* toxicity. With high stability, excellent biocompatibility, remarkable PDT efficacy, and efficient metabolism, COF nanodot-PEG represent a promising phototheranostic agent for advanced clinical tumor treatment.

Supramolecular self-assembly involves the spontaneous and orderly arrangement of molecules into nanoparticles through non-covalent interactions such as hydrogen bonding,  $\pi$ - $\pi$  stacking, electrostatic interactions, and hydrophobic effects, offering a promising approach for developing functional nanoparticles in biomedical applications.<sup>153,154</sup> Recently, researchers have developed several ultrasmall nanostructured PSs with renal-clearable properties using supramolecular self-assembly to enhance the safety of PDT. For instance, in 2023, Yang and colleagues synthesized a BODIPY derivative 1, functionalized with three triethylene glycol (TEG) chains and two pyridinium units (Fig. 13a).<sup>155</sup> By incorporating TEG arms and pyridinium moieties, the hydrophilicity, steric hindrance, and electrostatic repulsion of the resulting BODIPY derivative 1 were significantly increased, facilitating the self-assembly process to yield ultrasmall nanoparticles 1a with an average size of 5.6 nm. Intriguingly, the nano-assemblies 1a exhibited an 18.2-fold enhancement in ROS production capacity compared to the monomer in organic solution due to aggregation-increased ISC. Moreover, the dual-cationic property of nano-assemblies 1a, coupled with the higher negative membrane potential of cancer cells relative to normal cells, enhanced their tumor-targeting capability through electrostatic interactions. *In vivo* and *ex vivo* fluorescence imaging confirmed the specific accumulation of nano-assemblies 1a at tumor sites (signal-to-background ratio up to 11.5) and their rapid excretion *via* urinary processes, minimizing nonspecific accumulation in normal tissues. Exploiting these favorable characteristics, nano-assemblies 1a demonstrated effective PDT outcomes against cancer cells and solid tumors in preclinical models, with no observed toxicity to blood or major organs.

In 2024, Li and colleagues designed and synthesized a versatile dyad phthalocyanine molecule (PcSZ) based on the FRET mechanism (Fig. 13b).<sup>156</sup> Interestingly, PcSZ could spontaneously assemble into a uniform and stable nanosphere (NanoPcSZ) in aqueous solutions, with an average size of approximately 6 nm. Benefiting from the FRET effect, NanoPcSZ, a nanostructured type I PDT agent, exhibited enhanced

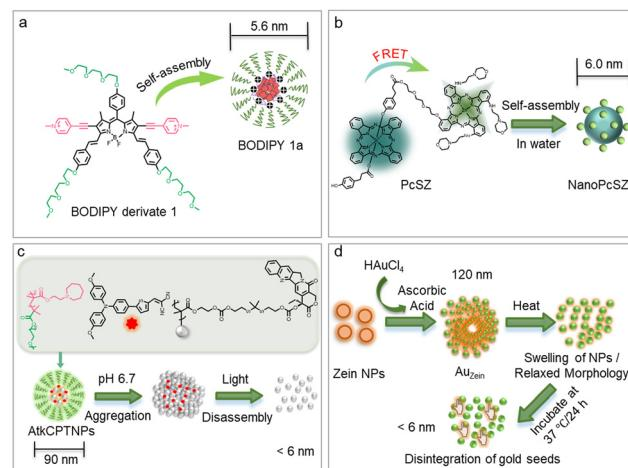


Fig. 13 (a) Schematic of the preparation of an ultrasmall nanotheranostic agent (BODIPY 1a) with renal-clearable properties *via* self-assembly. Reproduced with permission from ref. 155. Copyright, 2023, John Wiley & Sons. (b) Schematic of the preparation of an ultrasmall nanotheranostic agent (NanoPcSZ) with renal-clearable properties *via* self-assembly. Reproduced with permission from ref. 156. Copyright, 2024, John Wiley & Sons. (c) Schematic of a programmed size-changeable nanotheranostic agent for enhanced PDT and rapid elimination to prevent biotoxicity from drug accumulation. Reproduced with permission from ref. 159. Copyright, 2021, John Wiley & Sons. (d) Schematic of the synthesis and degradation of a renal-excretable gold core–shell nanotheranostic agent for improving PDT safety. Reproduced with permission from ref. 160. Copyright, 2023, Royal Society of Chemistry.

light-harvesting ability, leading to increased  $O_2^{\bullet-}$  production and heat generation upon NIR light exposure. These unique properties enabled NanoPcSZ to demonstrate excellent phototherapeutic effects under both normal and hypoxic conditions. NanoPcSZ exhibited obvious photocytotoxicity against mouse breast cancer (4T1) cells with a half maximal inhibitory concentration ( $IC_{50}$ ) of  $0.17 \pm 0.02 \mu\text{M}$  under hypoxic environments, which was 55-fold lower than that of the known PS methylene blue. In addition, both *in vivo* fluorescence and photoacoustic imaging confirmed NanoPcSZ's remarkable tumor accumulation capability. Finally, *in vivo* phototherapy significantly improved antitumor efficacy through a combination of photothermal action and type I photoreaction. Importantly, NanoPcSZ could be eliminated from organs (including the liver, lung, spleen, and kidney) other than the tumor site and excreted *via* urine within 24 h after systemic administration. This approach not only avoids potential drug accumulation biotoxicity but also enhances biosafety.

For renal-clearable nanostructure PSs, the ultrasmall particle size ( $< 6 \text{ nm}$ ) facilitates efficient renal excretion but diminishes the EPR effect. As a result, the drug may escape from the tumor region and re-enter the bloodstream, leading to reduced drug retention within the tumor.<sup>157</sup> Developing new smart nanostructure PSs that can change size before and after reaching tumor sites may mitigate this issue. Stimuli-responsive nanostructure PSs have been investigated to balance between tumor targeting for better therapeutic efficacy and renal clearance to reduce side effects. Zhou and colleagues



introduced CuSNDs, biodegradable and renal-clearable nanotheranostic platforms, consisting of doxorubicin-loaded biodegradable mesoporous silica nanoparticles (MSNs) for antitumor treatment.<sup>158</sup> These nanoparticles (MDNs) demonstrated a high tumor uptake due to prolonged circulation time. In addition, the MDNs exhibited photothermal-switchable drug release and a significant chemo-photothermal synergistic effect, validated in two preclinical models. The biodegradable MSNs allow rapid degradation of MDNs into ultrasmall nanoparticles, facilitating timely body excretion and preventing long-term toxicity. After treatment, the mice showed no significant abnormalities in body weight, food and water intake, grooming, activity, exploratory behavior, urination, or neurological status. Hematological and biochemical analyses revealed normal parameters, with no signs of infection or inflammatory responses. These results collectively indicated that MDNs possess high biocompatibility and biosafety.

In 2021, another type of programmed size-variable nanostructure theranostic agent (termed AktCPTNPs) based on AIE phototheranostic agent and polydrug-modified iron oxide nanoplates (IONPs) was fabricated by Wang *et al.* for improved chemo-photodynamic synergy therapy (Fig. 13c).<sup>159</sup> Initially, the nanostructure theranostic agent AktCPTNPs with an average size of approximately 90 nm can be enriched at tumor sites *via* passive targeting. However, in the mild acid tumor microenvironment, large particle sizes of IONPs were formed, achieving enhanced tumor accumulation. Under light exposure, the AIE phototheranostic agent generated abundant ROS for PDT and facilitated the release of the anticancer drug camptothecin, realizing a synergistic chemo/photodynamic effect. AktCPTNPs demonstrated excellent antitumor efficacy in mouse tumor models, and the survival rate of mice treated with AktCPTNPs was significantly increased. Importantly, following the therapy, the large-size nanostructure disintegrated into small-sized IONPs for rapid excretion from the body. This second-stage size transition (from large to small) enhances the metabolic clearance of IONPs, thereby reducing the risk of toxicity associated with long-term retention. This study not only presents an effective nanostructure theranostic agent for improved tumor treatment but also introduces a strategy for developing size-changeable nanostructure theranostic agents with enhanced tumor accumulation and high biosafety. Subsequently, Singh and co-workers synthesized a GSH-functionalized gold core–shell formulation ( $g\text{Au}_{\text{Zein}}$ ) with a particle size of approximately 120 nm using zein nanoparticles as templates (Fig. 13d).<sup>160</sup> Under laser irradiation,  $g\text{Au}_{\text{Zein}}$  generated ROS for PDT and heat for PTT. *In vitro* studies confirmed that both PDT and PTT induced by  $g\text{Au}_{\text{Zein}}$  resulted in cancer cell death. Remarkably, the heat produced by  $g\text{Au}_{\text{Zein}}$  facilitated its degradation into ultrasmall materials (<6 nm), which were subsequently eliminated from the body *via* urine. Furthermore, urine analysis after 24 hours post-injection showed minimal gold content, indicating efficient elimination of the degradation products of  $g\text{Au}_{\text{Zein}}$  from the body within 24 hours. Ultimately, the as-synthesized material demonstrated excellent efficacy as a theranostic agent in mouse models and exhibited non-toxicity for up to 14 days.

## 5. Conclusions: challenges and future prospects

Reviewing the evolution of PDT, enhancing the therapeutic effectiveness of PSs has consistently been a primary focus of scientific investigation. However, the sustainable progression of PDT and its clinical applications have also highlighted the significance of PDT biosafety. In this review, we summarize recent advances in enhancing PDT biosafety through PS design, such as creating activatable PSs to improve precision or developing degradable or metabolizable PSs that can promptly degrade or metabolize post-treatment to reduce drug accumulation. Responsive phototheranostic agents aim to enhance safety by increasing treatment specificity and accuracy. The activation strategies for these ROS-controllable PSs leverage known abnormalities in tumor tissues and cancer cells. These approaches have been previously utilized with diverse design methods, yielding positive results. In particular, dual activatable and reversible PSs have notably improved PDT safety. We expect that numerous innovative strategies based on multiple and reversible activations for smart PS development with high biosafety will continue to emerge in the future. Self-degradation and renal clearance post-treatment are intended to enhance safety by minimizing postoperative PS residues. We anticipate that self-degradable and renal-clearable strategies will be more widely adopted to create highly efficient PSs with good biosafety in the future. Particularly, nanostructure assemblies formed by self-assembly of single and pure molecular PSs with renal-clearable features should be promoted for further applications and potential clinical translation due to their relatively easier manufacturing process and potentially less toxicity. Several clinical trials of smart PSs for PDT have already begun, providing hope to patients.<sup>161,162</sup> For instance, laserphyrin (mono-L-aspartyl chlorine e6, NPe6) is a second-generation PS known for rapid clearance and low skin phototoxicity. Laserphyrin has shown significant clinical efficacy in treating early-stage lung cancer and has been on the market since June 2004.<sup>163</sup> In addition, 5-aminoketovaleric acid, a prodrug of porphyrin-based PSs, is widely used clinically due to its safety and cost-effectiveness.<sup>164</sup>

While the strategies for constructing PSs discussed herein have shown significant progress in enhancing the biosafety of PDT, there are still major challenges and issues that need systematic resolution to further advance PDT. First, the selectivity of existing responsive PSs to individual biomarkers is often inadequate. For instance, enzyme-responsive PSs struggle to selectively recognize different isoforms within the same enzyme family due to limitations in sensing mechanisms and reactive groups. Since the expression levels of isoforms are closely linked to disease types or progression, this limitation hinders the clinical translation of PDT. By applying the design principles of activatable fluorescent probes, innovating new recognition sites through molecular docking or inhibitor-mimicking techniques can significantly improve the development of responsive PSs, effectively addressing this challenge. Additionally, increasing the response threshold of activatable



PSs to tumor-specific biomarkers can ensure that activation occurs exclusively within tumor cells, thereby enhancing the safety of PDT. Furthermore, artificial intelligence emerges as a revolutionary tool, with the potential to rapidly and accurately generate new candidate structures with low toxicity and high photoactivity based on existing data of highly safe PS molecules, paving the way for advanced cancer therapies with enhanced safety. Moreover, artificial intelligence can assist in recommending the most appropriate type of PS, optimal dosage, and irradiation protocol based on existing high-safety PS molecular data. This personalized approach, guided by patient-specific information such as gene expression, lesion location, and immune status, aims to achieve maximum therapeutic efficacy while minimizing side effects. Second, research on degradable PSs is still in the early stages, and balancing degradability and treatment efficacy remains a challenge that requires significant attention. Furthermore, degradable PSs generate multiple metabolic byproducts when they are degraded in the body. In the future, systematic investigations on the *in vivo* distribution, metabolic pathways, and long-term toxicity of these byproducts should be strengthened. In addition, a more comprehensive biosafety evaluation system needs to be established to meet the regulatory requirements for clinical translation. Moreover, most reported light-triggered degradation strategies primarily rely on visible or first NIR light sources, which suffer from limited tissue penetration. In the future, novel degradable PSs responsive to NIR-II light, ultrasound, or X-ray irradiation could be developed to expand their applicability and safety in the treatment of deep-seated solid tumors. Third, PSs that can be cleared by the renal system are mostly composed of inorganic materials, often requiring complex building blocks and multi-step fabrication, which may limit their broader application. To promote wider application, it is recommended to use FDA-approved materials to enhance the safety of nanostructure theranostic agents. Furthermore, the scalability of nanomedicines is typically developed in small laboratory batches, and maintaining their performance during scale-up poses a significant challenge. Therefore, high priority should be placed on data sharing and establishing reliable, repeatable data standards to streamline processes, reduce costs, and save time. This review aims to provide a timely overview of the current status of this theme. The insights and discussions presented are expected to stimulate more research interest in developing more highly efficient and smart PSs to enhance the efficiency of PDT, reduce side effects, and improve safety, ultimately promoting the widespread clinical application of PDT.

## Conflicts of interest

There are no conflicts to declare.

## Data availability

No primary research results, software or code have been included and no new data were generated or analysed as part of this review.

## Acknowledgements

This work was supported by the Natural Science Foundation of China (Grant no. T2322004, X. Li), the Natural Science Foundation of China (Grant no. U21A20314, 22378100, and 22208087, H. Zhang), the Nano & Material Technology Development Program through the National Research Foundation of Korea (NRF) funded by Ministry of Science and ICT (RS-2024-00407093, J. Yoon) and the National Research Foundation of Korea (NRF) grant funded by the Korea government (MSIT) (No. 2022R1A2C3005420, J. Yoon).

## References

- 1 M. Piksa, C. Lian, I. C. Samuel, K. J. Pawlik, I. D. W. Samuel and K. Matczyszyn, *Chem. Soc. Rev.*, 2023, **52**, 1697–1722.
- 2 J. P. Celli, B. Q. Spring, I. Rizvi, C. L. Evans, K. S. Samkoe, S. Verma, B. W. Pogue and T. Hasan, *Chem. Rev.*, 2010, **110**, 2795–2838.
- 3 W. Fan, P. Huang and X. Chen, *Chem. Soc. Rev.*, 2016, **45**, 6488–6519.
- 4 X. Li, J. F. Lovell, J. Yoon and X. Chen, *Nat. Rev. Clin. Oncol.*, 2020, **17**, 657–674.
- 5 M. Li, Y. Xu, X. Peng and J. S. Kim, *Acc. Chem. Res.*, 2022, **55**, 3253–3264.
- 6 L. Huang, S. Zhao, J. Wu, L. Yu, N. Singh, K. Yang, M. Lan, P. Wang and J. S. Kim, *Coord. Chem. Rev.*, 2021, **438**, 213888.
- 7 S. Wang, L. Gai, Y. Chen, X. Ji, H. Lu and Z. Guo, *Chem. Soc. Rev.*, 2024, **53**, 3976–4019.
- 8 S. Monro, K. L. Colon, H. Yin, J. Roque, 3rd, P. Konda, S. Gujar, R. P. Thummel, L. Lilge, C. G. Cameron and S. A. McFarland, *Chem. Rev.*, 2019, **119**, 797–828.
- 9 W. Liu, S. He, X. Ma, C. Lv, H. Gu, J. Cao, J. Du, W. Sun, J. Fan and X. Peng, *Angew. Chem., Int. Ed.*, 2024, **63**, e202411802.
- 10 J. Zhang, X. Cao, H. Wen, Q. T. H. Shubhra, X. Hu, X. He and X. Cai, *Coord. Chem. Rev.*, 2025, **539**, 216746.
- 11 W. Zhou, Y. C. Liu, G. J. Liu, Y. Zhang, G. L. Feng and G. W. Xing, *Angew. Chem., Int. Ed.*, 2025, **64**, e202413350.
- 12 H. Hu, H. Wang, Y. Yang, J. F. Xu and X. Zhang, *Angew. Chem., Int. Ed.*, 2022, **61**, e202200799.
- 13 T. Zhu, J. Ding, F. Zheng, Y. Fang, W. Huang, Y. Yin and W. Zeng, *J. Med. Chem.*, 2025, **68**, 7630–7641.
- 14 M. Overchuk, R. A. Weersink, B. C. Wilson and G. Zheng, *ACS Nano*, 2023, **17**, 7979–8003.
- 15 Q. Tang, W. Xiao, C. Huang, W. Si, J. Shao, W. Huang, P. Chen, Q. Zhang and X. Dong, *Chem. Mater.*, 2017, **29**, 5216–5224.
- 16 Y. Wang, N. Gong, Y. Li, Q. Lu, X. Wang and J. Li, *J. Am. Chem. Soc.*, 2020, **142**, 1735–1739.
- 17 Y. Y. Zhao, L. Zhang, Z. Chen, B. Y. Zheng, M. Ke, X. Li and J. D. Huang, *J. Am. Chem. Soc.*, 2021, **143**, 13980–13989.
- 18 H. Kim, Y. R. Lee, H. Jeong, J. Lee, X. Wu, H. Li and J. Yoon, *Smart Mol.*, 2023, **1**, e20220010.



19 H. Gu, W. Sun, J. Du, J. Fan and X. Peng, *Smart Mol.*, 2023, **2**, e20230014.

20 Y. Gao, M. Xiong, C. Gong, B. Wang, L. Bai and X. B. Zhang, *Smart Mol.*, 2023, **1**, e20230014.

21 H. Zhou, D. Tang, Y. Yu, L. Zhang, B. Wang, J. Karges and H. Xiao, *Nat. Commun.*, 2023, **14**, 5350–5372.

22 H. Liu, Z. Li, X. Zhang, Y. Xu, G. Tang, Z. Wang, Y. Y. Zhao, M. R. Ke, B. Y. Zheng, S. Huang, J. D. Huang and X. Li, *Nat. Commun.*, 2025, **16**, 326–340.

23 L. Wu, Y. Liu, W. Zeng, Y. Ishigaki, S. Zhou, X. Wang, Y. Sun, Y. Zhang, X. Jiang, T. Suzuki and D. Ye, *J. Am. Chem. Soc.*, 2023, **145**, 27838–27849.

24 S. Yao, F. Xu, Y. Wang, J. Shang, S. Li, X. Xu, Z. Liu, W. He, Z. Guo and Y. Chen, *J. Am. Chem. Soc.*, 2025, **147**, 11132–11144.

25 T. C. Pham, V. N. Nguyen, Y. Choi, S. Lee and J. Yoon, *Chem. Rev.*, 2021, **121**, 13454–13619.

26 Y. Jiang, S. Huang, H. Ma, J. Weng, X. Du, Z. Lin, J. Kim, W. You, H. Zhang, D. Wang, J. S. Kim and H. Sun, *J. Am. Chem. Soc.*, 2024, **146**, 25270–25281.

27 X. Chen, L. Shi, X. Y. Ran, J. X. Xu, L. N. Zhang, Q. Q. Kong, X. Q. Yu and K. Li, *Adv. Funct. Mater.*, 2024, **34**, 2400728.

28 X. Chen, B. B. Mendes, Y. Zhuang, J. Connio, S. Mercado Argandona, F. Melle, D. P. Sousa, D. Perl, A. Chivu, H. K. Patra, W. Shepard, J. Conde and D. Fairen-Jimenez, *J. Am. Chem. Soc.*, 2024, **146**, 1644–1656.

29 V. N. Nguyen, S. Qi, S. Kim, N. Kwon, G. Kim, Y. Yim, S. Park and J. Yoon, *J. Am. Chem. Soc.*, 2019, **141**, 16243–16248.

30 Y. Y. Zhao, X. Zhang, Z. Chen, Y. Xu, H. Kim, H. Jeong, Y. R. Lee, J. Lee, X. Li and J. Yoon, *Aggregate*, 2024, **5**, e514.

31 Y. Zou, S. Long, T. Xiong, X. Zhao, W. Sun, J. Du, J. Fan and X. Peng, *ACS Cent. Sci.*, 2021, **7**, 327–334.

32 J. Wang, P. Shangguan, M. Lin, L. Fu, Y. Liu, L. Han, S. Chen, X. Wang, M. Lu, Z. Luo, Y. Zhong, B. Shi and F. Bai, *ACS Nano*, 2023, **17**, 16840–16853.

33 J. Zou, Z. Yin, K. Ding, Q. Tang, J. Li, W. Si, J. Shao, Q. Zhang, W. Huang and X. Dong, *ACS Appl. Mater. Interfaces*, 2017, **9**, 32475–32481.

34 Q. Jiang, J. Li, Z. Du, M. Li, L. Chen, X. Zhang, X. Tang, Y. Shen, D. Ma, W. Li, L. Li, N. Alifu, Q. Hu and J. Liu, *Adv. Healthcare Mater.*, 2024, **13**, 2400962.

35 Z. Fan, K. X. Teng, Y. Y. Xu, L. Y. Niu and Q. Z. Yang, *Angew. Chem., Int. Ed.*, 2025, **64**, e202413595.

36 Y. Xu, D. An, T. Zhang, X. Wu, S. Wang, J. Shao, L. L. Qu, Y. Guo and X. Dong, *Adv. Mater.*, 2025, **37**, 2418894.

37 S. Zeng, Y. Wang, C. Chen, H. Kim, X. Liu, M. Jiang, Y. Yu, Y. S. Kafuti, Q. Chen, J. Wang, X. Peng, H. Li and J. Yoon, *Angew. Chem., Int. Ed.*, 2024, **63**, e202316487.

38 X. Li, S. Yu, Y. Lee, T. Guo, N. Kwon, D. Lee, S. C. Yeom, Y. Cho, G. Kim, J. D. Huang, S. Choi, K. T. Nam and J. Yoon, *J. Am. Chem. Soc.*, 2019, **141**, 1366–1372.

39 M. R. Younis, G. He, J. Qu, J. Lin, P. Huang and X. H. Xia, *Adv. Sci.*, 2021, **8**, 2102587.

40 S. Li, K. Gu, H. Wang, B. Xu, H. Li, X. Shi, Z. Huang and H. Liu, *J. Am. Chem. Soc.*, 2020, **142**, 5649–5656.

41 S. Pinel, N. Thomas, C. Boura and M. Barberi-Heyob, *Adv. Drug. Delivery Rev.*, 2019, **138**, 344–357.

42 M. Zhang, M. Lu, Y. Gong, Y. Yang, J. Song, J. Li, Z. Chen, Y. Ling and Y. Zhou, *Small*, 2024, **20**, 2400587.

43 Y.-Y. Zhao, H. Kim, V.-N. Nguyen, S. Jang, W. Jun Jang and J. Yoon, *Coord. Chem. Rev.*, 2024, **501**, 215560.

44 P. C. Lo, M. S. Rodriguez-Morgade, R. K. Pandey, D. K. P. Ng, T. Torres and F. Dumoulin, *Chem. Soc. Rev.*, 2020, **49**, 1041–1056.

45 H. B. Cheng, X. Cao, S. Zhang, K. Zhang, Y. Cheng, J. Wang, J. Zhao, L. Zhou, X. J. Liang and J. Yoon, *Adv. Mater.*, 2023, **35**, 2207546.

46 J. Yuan, H. Yang, W. Huang, S. Liu, H. Zhang, X. Zhang and X. Peng, *Chem. Soc. Rev.*, 2025, **54**, 341–366.

47 Y. Duo, L. Han, Y. Yang, Z. Wang, L. Wang, J. Chen, Z. Xiang, J. Yoon, G. Luo and B. Z. Tang, *Chem. Rev.*, 2024, **124**, 11242–11347.

48 Y. Y. Zhao, B. Hwang, Y. Lee and J. Yoon, *Nat. Sci. Rev.*, 2024, **11**, nwae048.

49 Y.-Y. Zhao, J.-Y. Chen, J.-Q. Hu, L. Zhang, A.-L. Lin, R. Wang, B.-Y. Zheng, M.-R. Ke, X. Li and J.-D. Huang, *Dyes Pigm.*, 2021, **189**, 109270.

50 X. Yang, M. He, Y. Li, T. Qiu, J. Zuo, Y. Jin, J. Fan, W. Sun and X. Peng, *J. Mater. Chem. B*, 2024, **12**, 7113–7121.

51 Z. Zeng, C. Zhang, J. Li, D. Cui, Y. Jiang and K. Pu, *Adv. Mater.*, 2021, **33**, 2007247.

52 L. Jiang, H. Bai, L. Liu, F. Lv, X. Ren and S. Wang, *Angew. Chem., Int. Ed.*, 2019, **58**, 10660–10665.

53 T. Luo, Y. Fan, J. Mao, E. Yuan, E. You, Z. Xu and W. Lin, *J. Am. Chem. Soc.*, 2022, **144**, 5241–5246.

54 W. Wang, C. Zhu, B. Zhang, Y. Feng, Y. Zhang and J. Li, *J. Am. Chem. Soc.*, 2023, **145**, 16642–16649.

55 K. Wei, Y. Wu, X. Zheng, L. Ouyang, G. Ma, C. Ji and M. Yin, *Angew. Chem., Int. Ed.*, 2024, **63**, e202404395.

56 L. K. B. Tam and D. K. P. Ng, *Mater. Chem. Front.*, 2023, **7**, 3184–3193.

57 Z. Li, Z. Zhou, Y. Wang, J. Wang, L. Zhou, H.-B. Cheng and J. Yoon, *Coord. Chem. Rev.*, 2023, **493**, 215324.

58 B. M. Luby, C. D. Walsh and G. Zheng, *Angew. Chem., Int. Ed.*, 2019, **58**, 2558–2569.

59 P. Cheng and K. Pu, *Nat. Rev. Mater.*, 2021, **6**, 1095–1113.

60 J. Huang, X. Chen, Y. Jiang, C. Zhang, S. He, H. Wang and K. Pu, *Nat. Mater.*, 2022, **21**, 598–607.

61 X. Li, S. Kolemen, J. Yoon and E. U. Akkaya, *Adv. Funct. Mater.*, 2017, **27**, 1604053.

62 L. Wu, J. Huang, K. Pu and T. D. James, *Nat. Rev. Chem.*, 2021, **5**, 406–421.

63 T. J. Dougherty, M. T. Cooper and T. S. Mang, *Lasers Surg. Med.*, 1990, **10**, 485–488.

64 Highlights of prescribing information: Photofrin (porfimer sodium) injection. [https://www.accessdata.fda.gov/drugsatfda\\_docs/label/2011/020451s020lbl.pdf](https://www.accessdata.fda.gov/drugsatfda_docs/label/2011/020451s020lbl.pdf) (accessed December 24, 2022).

65 A. L. Harris, *Nat. Rev. Cancer*, 2002, **2**, 38–47.

66 J. N. Liu, W. Bu and J. Shi, *Chem. Rev.*, 2017, **117**, 6160–6224.



67 B. A. Webb, M. Chimenti, M. P. Jacobson and D. L. Barber, *Nat. Rev. Cancer*, 2011, **11**, 671–677.

68 X. Zhang, Y. Lin and R. J. Gillies, *J. Nucl. Med.*, 2010, **51**, 1167–1170.

69 E. Nestoros, A. Sharma, E. Kim, J. S. Kim and M. Vendrell, *Nat. Rev. Chem.*, 2025, **9**, 46–60.

70 S. R. Punganuru, H. R. Madala, V. Arutla and K. S. Srivenugopal, *Cancers*, 2018, **10**, 470–484.

71 K. Li, W. Dong, L. Qiu, Q. Liu, G. Lv, Y. Peng, M. Xie and J. Lin, *Eur. J. Med. Chem.*, 2019, **181**, 111582.

72 Q. Zeng, R. Zhang, T. Zhang and D. Xing, *Biomaterials*, 2019, **207**, 39–48.

73 G. Ma, Z. Liu, C. Zhu, H. Chen, R. T. K. Kwok, P. Zhang, B. Z. Tang, L. Cai and P. Gong, *Angew. Chem., Int. Ed.*, 2022, **61**, e202207213.

74 M. R. Albertella, P. M. Loadman, P. H. Jones, R. M. Phillips, R. Rampling, N. Burnet, C. Alcock, A. Anthoney, E. Vjaters, C. R. Dunk, P. A. Harris, A. Wong, A. S. Lalani and C. J. Twelves, *Clin. Cancer Res.*, 2008, **14**, 1096–1104.

75 A. Sharma, J. F. Arambula, S. Koo, R. Kumar, H. Singh, J. L. Sessler and J. S. Kim, *Chem. Soc. Rev.*, 2019, **48**, 771–813.

76 S. Takahashi, W. Piao, Y. Matsumura, T. Komatsu, T. Ueno, T. Terai, T. Kamachi, M. Kohno, T. Nagano and K. Hanaoka, *J. Am. Chem. Soc.*, 2012, **134**, 19588–19591.

77 W. Piao, K. Hanaoka, T. Fujisawa, S. Takeuchi, T. Komatsu, T. Ueno, T. Terai, T. Tahara, T. Nagano and Y. Urano, *J. Am. Chem. Soc.*, 2017, **139**, 13713–13719.

78 S. Zhou, X. Hu, R. Xia, S. Liu, Q. Pei, G. Chen, Z. Xie and X. Jing, *Angew. Chem., Int. Ed.*, 2020, **59**, 23198–23205.

79 J. Xiong, P. Wang, S. Son, C. Zhong, F. Zhang, Z. Mao, Z. Liu and J. S. Kim, *Matter*, 2022, **5**, 1502–1519.

80 Y. Y. Zhao, Y. Xu, X. Zhang, Z. Chen, H. Kim, X. Li and J. Yoon, *Angew. Chem., Int. Ed.*, 2025, **64**, e202506412.

81 J. Liu, A. Wang, S. Liu, R. Yang, L. Wang, F. Gao, H. Zhou, X. Yu, J. Liu and C. Chen, *Angew. Chem., Int. Ed.*, 2021, **60**, 25328–25338.

82 C. Lu, C. Zhang, P. Wang, Y. Zhao, Y. Yang, Y. Wang, H. Yuan, S. Qu, X. Zhang, G. Song and K. Pu, *Chem*, 2020, **6**, 2314–2334.

83 P. Montcourrier, I. Silver, R. Farnoud, I. Bird and H. Rochefort, *Clin. Exp. Metastasis*, 1997, **15**, 382–392.

84 J. Zou, P. Wang, Y. Wang, G. Liu, Y. Zhang, Q. Zhang, J. Shao, W. Si, W. Huang and X. Dong, *Chem. Sci.*, 2019, **10**, 268–276.

85 Y. Liu, J. Zhang, X. Zhou, Y. Wang, S. Lei, G. Feng, D. Wang, P. Huang and J. Lin, *Angew. Chem., Int. Ed.*, 2024, **63**, e202408064.

86 Y. Liu, Y. Li, W. Sun, Z. Sun, Y. Wang, S. Lei, P. Huang and J. Lin, *Anal. Chem.*, 2025, **97**, 3310–3318.

87 B. Sun, R. Chang, S. Cao, C. Yuan, L. Zhao, H. Yang, J. Li, X. Yan and J. C. M. van Hest, *Angew. Chem., Int. Ed.*, 2020, **59**, 20582–20588.

88 M. H. Lee, J. L. Sessler and J. S. Kim, *Acc. Chem. Res.*, 2015, **48**, 2935–2946.

89 Z. Fu, D. Zhou, Z. Liu and D. Ni, *Coord. Chem. Rev.*, 2025, **533**, 216554.

90 Y. Wang, S. Xu, L. Shi, C. Teh, G. Qi and B. Liu, *Angew. Chem., Int. Ed.*, 2021, **60**, 14945–14953.

91 J. Sun, X. Cai, C. Wang, K. Du, W. Chen, F. Feng and S. Wang, *J. Am. Chem. Soc.*, 2021, **143**, 868–878.

92 R. Wang, X. Xia, Y. Yang, X. Rong, T. Liu, Z. Su, X. Zeng, J. Du, J. Fan, W. Sun and X. Peng, *Adv. Healthcare Mater.*, 2022, **11**, 2102017.

93 Y. Liu, Y. Yao, J. Sha, G. Liang and X. Sun, *ACS Biomater. Sci. Eng.*, 2025, **11**, 730–741.

94 J. Lv, R. Yue, H. Liu, H. Du, C. Lu, C. Zhang, G. Guan, S. Min, S. Huan, H. Kang and G. Song, *Coord. Chem. Rev.*, 2024, **510**, 215842.

95 B. Zhang, D. Lu, D. B. R. Wang, Z. Y. Kok, M. B. Chan-Park and H. Duan, *Adv. Funct. Mater.*, 2024, **34**, 2407869.

96 A. Loktev, T. Lindner, W. Mier, J. Debus, A. Altmann, D. Jager, F. Giesel, C. Kratochwil, P. Barthe, C. Roumestand and U. Haberkorn, *J. Nucl. Med.*, 2018, **59**, 1423–1429.

97 H. Zhou, Y. Zhang, R. Zhang, M. Zhao, W. Chen, Y. Liu, Y. Jiang, Q. Li, Q. Miao and M. Gao, *Adv. Mater.*, 2023, **35**, 2211485.

98 M. Zhao, Y. Zhang, J. Miao, H. Zhou, Y. Jiang, Y. Zhang, M. Miao, W. Chen, W. Xing, Q. Li and Q. Miao, *Adv. Mater.*, 2024, **36**, 2305243.

99 F. M. Barnieh, P. M. Loadman and R. A. Falconer, *Biochim. Biophys. Acta, Rev. Cancer*, 1876, **2021**, 188641.

100 Y. Liu, J. Zeng, Q. Li, M. Miao, Z. Song, M. Zhao, Q. Miao and M. Gao, *Adv. Optical Mater.*, 2022, **10**, 2102709.

101 X. Shi, Y. Deng, X. Liu, G. Gao, R. Wang and G. Liang, *Biosens. Bioelectron.*, 2022, **208**, 114212.

102 X. Hu, F. Li, S. Wang, F. Xia and D. Ling, *Adv. Healthcare Mater.*, 2018, **7**, 1800359.

103 Y. Wang, H. Xu and X. Zhang, *Adv. Mater.*, 2009, **21**, 2849–2864.

104 X. Li, C. Y. Kim, S. Lee, D. Lee, H. M. Chung, G. Kim, S. H. Heo, C. Kim, K. S. Hong and J. Yoon, *J. Am. Chem. Soc.*, 2017, **139**, 10880–10886.

105 Y. Cai, D. Ni, W. Cheng, C. Ji, Y. Wang, K. Mullen, Z. Su, Y. Liu, C. Chen and M. Yin, *Angew. Chem., Int. Ed.*, 2020, **59**, 14014–14018.

106 L. Xu, H. Gao, W. Zhan, Y. Deng, X. Liu, Q. Jiang, X. Sun, J. J. Xu and G. Liang, *J. Am. Chem. Soc.*, 2023, **145**, 27748–27756.

107 Y. Hu, J. Liu, M. Xu and K. Pu, *J. Am. Chem. Soc.*, 2025, **147**, 7148–7157.

108 K. X. Teng, L. Y. Niu, Y. F. Kang and Q. Z. Yang, *Chem. Sci.*, 2020, **11**, 9703–9711.

109 Y. Fu, M. S. Jang, N. Wang, Y. Li, T. P. Wu, J. H. Lee, D. S. Lee and H. Y. Yang, *J. Controlled Release*, 2020, **327**, 129–139.

110 J. Zou, Z. Li, Y. Zhu, Y. Tao, Q. You, F. Cao, Q. Wu, M. Wu, J. Cheng, J. Zhu and X. Chen, *Bioact. Mater.*, 2024, **34**, 414–421.

111 D. Tokura, K. Konarita, M. Suzuki, K. Ogata, Y. Honda, Y. Miura, N. Nishiyama and T. Nomoto, *J. Control. Release*, 2024, **371**, 445–454.



112 Y. Xiang, B. Wang, W. Yang, X. Zheng, R. Chen, Q. Gong, Z. Gu, Y. Liu and K. Luo, *Adv. Mater.*, 2024, **36**, 2311500.

113 H. Zhang, M. Cui, D. Tang, B. Wang, G. Liang, C. Xu and H. Xiao, *Adv. Mater.*, 2024, **36**, 2310298.

114 L. Chen, W. Zhuang, C. Hu, T. Yu, X. Su, Z. Liang, G. Li and Y. Wang, *J. Mater. Chem. B*, 2020, **8**, 5645–5654.

115 N. Zhang, D. Wang, X. Jing, T. Yang, H. Yang and L. Meng, *ACS Appl. Bio. Mater.*, 2021, **4**, 6294–6303.

116 J. S. Bond, *J. Biol. Chem.*, 2019, **294**, 1643–1651.

117 M. Vizovisek, D. Ristanovic, S. Menghini, M. G. Christiansen and S. Schuerle, *Int. J. Mol. Sci.*, 2021, **22**, 2514–2543.

118 X. Wei, C. Zhang, S. He, J. Huang, J. Huang, S. S. Liew, Z. Zeng and K. Pu, *Angew. Chem., Int. Ed.*, 2022, **61**, e202202966.

119 L. K. B. Tam, L. Yu, R. C. H. Wong, W. P. Fong, D. K. P. Ng and P. C. Lo, *J. Med. Chem.*, 2021, **64**, 17455–17467.

120 L. K. B. Tam, J. C. H. Chu, L. He, C. Yang, K. C. Han, P. C. K. Cheung, D. K. P. Ng and P. C. Lo, *J. Am. Chem. Soc.*, 2023, **145**, 7361–7375.

121 J. C. H. Chu, C. T. T. Wong and D. K. P. Ng, *Angew. Chem., Int. Ed.*, 2023, **62**, e202214473.

122 W. Hu, T. He, H. Zhao, H. Tao, R. Chen, L. Jin, J. Li, Q. Fan, W. Huang, A. Baev and P. N. Prasad, *Angew. Chem., Int. Ed.*, 2019, **58**, 11105–11111.

123 P. Xiao, W. Xie, J. Zhang, Q. Wu, Z. Shen, C. Guo, Y. Wu, F. Wang, B. Z. Tang and D. Wang, *J. Am. Chem. Soc.*, 2023, **145**, 334–344.

124 Y. Chai, Y. Sun, Z. Sheng, Y. Zhu, T. Du, B. Zhu, H. Yu, B. Dong, Y. Liu and H. Y. Wang, *Acta Biomater.*, 2024, **188**, 315–328.

125 J. Tian, B. Li, F. Zhang, Z. Yao, W. Song, Y. Tang, Y. Ping and B. Liu, *Angew. Chem., Int. Ed.*, 2023, **62**, e202307288.

126 D. Zhang, K. X. Teng, N. Shao, L. Y. Niu and Q. Z. Yang, *J. Med. Chem.*, 2025, **68**, 8648–8658.

127 T. G. Chen, X. Q. Zhang, J. F. Ge, Y. J. Xu and R. Sun, *Spectrochim. Acta, Part A*, 2022, **270**, 120783.

128 B. Yuan, H. Wu, H. Wang, B. Tang, J. F. Xu and X. Zhang, *Angew. Chem., Int. Ed.*, 2021, **60**, 706–710.

129 H. Huang, W. Xie, Q. Wan, L. Mao, D. Hu, H. Sun, X. Zhang and Y. Wei, *Adv. Sci.*, 2022, **9**, 2104101.

130 H. Huang, W. Xie, D. Hu, X. He, R. Li, X. Zhang and Y. Wei, *Chem. Eng. J.*, 2023, **451**, 138617.

131 Y. Li, P. Zhang, Y. Xie, J. Yang, Y. Yang, L. Shi, W. Wu and Z. Li, *Biomaterials*, 2023, **299**, 122182.

132 M. Klaper, P. Wessig and T. Linker, *Chem. Commun.*, 2016, **52**, 1210–1213.

133 J. Gao, H. Yang, Y. Lu, Q. Shi, S. Xu, W. Wu, F. Hu and B. Liu, *Chem. Mater.*, 2023, **35**, 1229–1237.

134 Y.-Y. Zhao, Z. Chen, L. Zhang, X.-W. Qin, H. Liu, B.-Y. Zheng, M. Ke, J.-D. Huang and X. Li, *Chem. Eng. J.*, 2023, **474**, 145921.

135 H. Lee, J. Kim, J. Lee, H. Park, Y. Park, S. Jung, J. Lim, H. C. Choi and W. J. Kim, *Biomaterials*, 2020, **263**, 120402.

136 J. Shi, Z. Wang, C. Shen, T. Pan, L. Xie, M. Xie, L. Huang, Y. Jiang, J. Zhou, W. Zuo and Z.-S. Huang, *Dyes Pigm.*, 2022, **200**, 110122.

137 H. S. Choi, W. Liu, P. Misra, E. Tanaka, J. P. Zimmer, B. Itty Ipe, M. G. Bawendi and J. V. Frangioni, *Nat. Biotechnol.*, 2007, **25**, 1165–1170.

138 J. Liu, M. Yu, C. Zhou and J. Zheng, *Mater. Today*, 2013, **16**, 477–486.

139 M. Longmire, P. L. Choyke and H. Kobayashi, *Nanomedicine*, 2008, **3**, 703–717.

140 M. Ferrari, *Nat. Rev. Cancer*, 2005, **5**, 161–171.

141 W. Fan, B. Yung, P. Huang and X. Chen, *Chem. Rev.*, 2017, **117**, 13566–13638.

142 J. Ouyang, A. Xie, J. Zhou, R. Liu, L. Wang, H. Liu, N. Kong and W. Tao, *Chem. Soc. Rev.*, 2022, **51**, 4996–5041.

143 A. Nel, T. Xia, L. Mädler and N. Li, *Science*, 2006, **311**, 622–627.

144 C. H. Choi, J. E. Zuckerman, P. Webster and M. E. Davis, *Proc. Natl. Acad. Sci. U. S. A.*, 2011, **108**, 6656–6661.

145 B. Du, X. Jiang, A. Das, Q. Zhou, M. Yu, R. Jin and J. Zheng, *Nat. Nanotechnol.*, 2017, **12**, 1096–1102.

146 Q. Weng, H. Sun, C. Fang, F. Xia, H. Liao, J. Lee, J. Wang, A. Xie, J. Ren, X. Guo, F. Li, B. Yang and D. Ling, *Nat. Commun.*, 2021, **12**, 1436–1449.

147 T. Guo, Y. Wu, Y. Lin, X. Xu, H. Lian, G. Huang, J. Z. Liu, X. Wu and H. H. Yang, *Small*, 2018, **14**, 1702815.

148 L. Yang, Y. Liu, X. Ren, R. Jia, L. Si, J. Bao, Y. Shi, J. Sun, Y. Zhong, P. C. Duan, X. Yang, R. Zhu, Y. Jia and F. Bai, *ACS Nano*, 2024, **18**, 3161–3172.

149 C. Deng, M. Zheng, S. Han, Y. Wang, J. Xin, O. Aras, L. Cheng and F. An, *Adv. Funct. Mater.*, 2023, **33**, 2300348.

150 L. Cheng, D. Jiang, A. Kamkaew, H. F. Valdovinos, H. J. Im, L. Feng, C. G. England, S. Goel, T. E. Barnhart, Z. Liu and W. Cai, *Adv. Funct. Mater.*, 2017, **27**, 1702928.

151 K. Siyawannapong, R. Zhang, H. Lei, Q. Jin, W. Tang, Z. Dong, R. Y. Lai, Z. Liu, A. Kamkaew and L. Cheng, *Theranostics*, 2020, **10**, 62–73.

152 Y. Zhang, L. Zhang, Z. Wang, F. Wang, L. Kang, F. Cao, K. Dong, J. Ren and X. Qu, *Biomaterials*, 2019, **223**, 119462.

153 H. Zhu, H. Wang, B. Shi, L. Shangguan, W. Tong, G. Yu, Z. Mao and F. Huang, *Nat. Commun.*, 2019, **10**, 2412–2421.

154 Y. Liu, H. Wang, S. Li, C. Chen, L. Xu, P. Huang, F. Liu, Y. Su, M. Qi, C. Yu and Y. Zhou, *Nat. Commun.*, 2020, **11**, 1724–1735.

155 D. Zhang, K. X. Teng, L. Zhao, L. Y. Niu and Q. Z. Yang, *Adv. Mater.*, 2023, **35**, 2209789.

156 Y. Y. Zhao, X. Zhang, Y. Xu, Z. Chen, B. Hwang, H. Kim, H. Liu, X. Li and J. Yoon, *Angew. Chem., Int. Ed.*, 2024, **63**, e202411514.

157 P. Zhao, S. Liu, L. Wang, G. Liu, Y. Cheng, M. Lin, K. Sui and H. Zhang, *Carbohydr. Polym.*, 2020, **241**, 116344.

158 Q. Wei, Y. Chen, X. Ma, J. Ji, Y. Qiao, B. Zhou, F. Ma, D. Ling, H. Zhang, M. Tian, J. Tian and M. Zhou, *Adv. Funct. Mater.*, 2018, **28**, 1704634.

159 G. Cheng, W. Zong, H. Guo, F. Li, X. Zhang, P. Yu, F. Ren, X. Zhang, X. Shi, F. Gao, J. Chang and S. Wang, *Adv. Mater.*, 2021, **33**, 2100398.

160 B. Singh, C. Patnaik, R. Bahadur, M. Gandhi, A. De and R. Srivastava, *Nanoscale*, 2023, **15**, 1273–1288.



161 N. Sekkat, H. van den Bergh, T. Nyokong and N. Lange, *Molecules*, 2011, **17**, 98–144.

162 E. D. Baron, C. L. Malbasa, D. Santo-Domingo, P. Fu, J. D. Miller, K. K. Hanneman, A. H. Hsia, N. L. Oleinick, V. C. Colussi and K. D. Cooper, *Lasers Surg. Med.*, 2010, **42**, 728–735.

163 K. Furuse, M. Fukuoka, H. Kato, T. Horai, K. Kubota, N. Kodama, Y. Kusunoki, N. Takifuji, T. Okunaka, C. Konaka, H. Wada and Y. Hayata, *J. Clin. Oncol.*, 1993, **11**, 1852–1857.

164 L. Shi, H. Wang, K. Chen, J. Yan, B. Yu, S. Wang, R. Yin, X. Nong, X. Zou, Z. Chen, C. Li, L. Chen, C. Zhang, F. Zhang, H. Zheng, M. Zheng, P. Tu, J. Xu, J. Tao, X. Kang, K. Zeng, Y. Lu, N. Yu, X. Lei, M. Pan, Q. Ju, H. Gu and X. Wang, *Photodiagn. Photodyn. Ther.*, 2021, **35**, 102340.

